12-2013

CHARACTERIZATION OF HEAT TRANSFER COEFFICIENT UNCERTAINTY IN SUPPORT OF HIGH TEMPERATURE PROBE MEASUREMENT TECHNOLOGY

Marcus S. Conner
University of Tennessee - Knoxville, marcus.conner@arnold.af.mil

To the Graduate Council:

I am submitting herewith a thesis written by Marcus S. Conner entitled "CHARACTERIZATION OF HEAT TRANSFER COEFFICIENT UNCERTAINTY IN SUPPORT OF HIGH TEMPERATURE PROBE MEASUREMENT TECHNOLOGY." I have examined the final electronic copy of this thesis for form and content and recommend that it be accepted in partial fulfillment of the requirements for the degree of Master of Science, with a major in Mechanical Engineering.

Trevor Moller, Major Professor

We have read this thesis and recommend its acceptance:

Monty Smith, Feng-Yuan Zhang

Accepted for the Council:
Carolyn R. Hodges

Vice Provost and Dean of the Graduate School

(Original signatures are on file with official student records.)

CHARACTERIZATION OF HEAT TRANSFER COEFFICIENT UNCERTAINTY IN SUPPORT OF HIGH TEMPERATURE PROBE MEASUREMENT TECHNOLOGY

A Thesis Presented for the

Master of Science

Degree

The University of Tennessee, Knoxville

MARCUS S. CONNER

DECEMBER 2013

ACKNOWLEDGMENTS

I would like to express my deep gratitude to Dr. Trevor Moeller and Mr. Bob Rhodes for their support and guidance while working on this topic. The work described within this document would not have been possible without them and has provided me with knowledge and tools that I have benefited greatly from in my occupation working at Arnold Engineering Development Center (AEDC). I would also like to thank Ms. Sabrina Hurlock and Ms. Erin Halpenny for their contributions to the uncertainty analysis described within this document, and Dr. Montgomery Smith and Dr. Feng-Yuan Zhang for serving on my committee. Most importantly I would like to thank my wonderful wife for the patience and support that without, I most certainty would not have been able to make it to where I am today.

I would also like it to be known that the majority of the testing and the development of the heat transfer relationships were a collaborative effort between UTSI (Dr. Moeller, Mr. Rhodes, Mr. Joel Davenport) and myself. In addition to the previous efforts I have conducted an analysis into the validity of the results. Both the development and validation results are discussed in this thesis.

ABSTRACT

The development of new materials and processes have enabled defense, industrial, and research devices that operate in high temperature environments. Measurement technology must keep up with the demand of these environments.

The objective of this work is to provide a correlation between the heat transfer coefficient (and Nusselt Number) and the flow Reynolds number (and Prandtl number) for the tip region of a truncated cylindrical probe. The correlation provides reduced uncertainty for materials whose heat transfer coefficient is not well defined. The configuration for the experiment uses the University of Tennessee Space Institute's (UTSI) blow down air supply system discharging into a duct and exhausting to atmosphere. This system provides dry pressurized air that is thermally stabilized to the test section. The test article is a heated probe that is instrumented with thermocouples. Experimental data were recorded for many run conditions. These data were utilized to develop the correlation between the probe tip heat transfer coefficient and the Reynolds number.

As a result of the work presented in the body of this text, a correlation between the heat transfer coefficient and the Reynolds number was developed with an uncertainty of 1.24%.

TABLE OF CONTENTS

LIST OF TABLES

LIST OF FIGURES

1 INTRODUCTION

The objective of this work is to provide a correlation between the heat transfer coefficient (and Nusselt number) and the flow Reynolds number (and Prandtl number) for a truncated cylindrical probe in cross flow. The temperature probe is a low temperature replica of a similar probe being designed for high temperature applications. A missing piece of the high temperature probe design process was the probe tip heat transfer coefficient. This research was conducted to fill this gap in knowledge. There are no Nusselt number correlations for this configuration reported in the literature.

Normally, the correlation uses the Nusselt number (hd/k), and in the simplest form is proportional to the product of the Reynolds and Prandtl numbers, each raised to some power (Bergman, Dewitt, Incropera, & Lavine, 2011). The gas properties used in Nusselt number correlations are often those at the average of the temperature of the gas and the surface of the body to which the heat is being transferred. The experiments in the tests do not have any significant variation in Prandtl number, and the correlation with Nusselt number assumes the functional form from a similar geometry.

The Reynolds number (Gd/μ) may be defined in various ways. The preferred choice for this application is to use the total mass flow and the duct area to define the mass flux (G), as opposed to a local velocity and density, since this is the only information that will be available during the testing with the high temperature probe in the targeted flow environments. The viscosity (μ) is evaluated at the gas total temperature. The probe diameter is used as the characteristic length (d).

The correlation described above will provide overall heat transfer coefficients for a short cylinder projecting into an air flow at Reynolds numbers from 30,000 to 150,000. The range of Prandtl numbers of the heated, high pressure air to be used with the high

temperature probe, calculated with the NASA CEA code (Gordon & McBride, 1994), was found to vary between 0.70 and 0.75. The tests described herein were run with air at a Prandtl number of about 0.71, so it is expected that determining the Nusselt number as a function of Reynolds number only will be sufficient to account for the test flow properties. Since the diameter of the test probe is fixed and the change in viscosity is small, the majority of the Reynolds number change in these tests results from a change in air velocity and its turbulence intensity level. The Nusselt number correlation ultimately determined in this work will provide a means of calculating the convective heat transfer coefficient for flows with different gas properties as a function of Reynolds number and Prandtl number.

The experimental configuration is an aluminum cylinder heated internally with a cartridge heater and uses air flow to extract heat from the tip. It is noteworthy that some heat transfer Nusselt numbers have a form that depends slightly on whether heat is input to a surface or extracted from a surface for the same heat transfer ΔT. For turbulent duct and pipe flow heat transfer, the effect of heating or cooling is expressed in the Dittus-Boelter Nusselt Number in the exponent of the Prandtl number, e.g., $Pr^{0.3}$ vs. $Pr^{0.4}$, for heating the wall versus cooling the wall, respectively (Bergman, Dewitt, Incropera, & Lavine, 2011). For turbulent air in a duct flow, this amounts to a difference of 3.4% in the predicted Nusselt number. The majority of other heat transfer Nusselt numbers for gas flow heat transfer use $Pr^{0.3\text{-}0.33}$ as the Prandtl number factor.

2 TESTING PHASE

2.1 FACILITY

The experiment configuration shown in Figure 1 uses the UTSI blow down air supply system discharging into a 36 inch long, 6 inch diameter duct and exhausting to atmosphere. The probe is supported by a modified compression fitting located 18.5 inches (3 pipe diameters) downstream of the inlet. This configuration establishes the velocity profile shapes and turbulence levels in the pipe sections containing the high temperature probe, and is similar to the environment in which a high temperature probe would be used. Two pressure taps are located on the wall of the duct, opposite the probe, 6 inches upstream and 6 inches downstream of the probe station. These taps are used to obtain the static pressure in the duct and as holders for the total pressure and hot wire probe used for flow characterization. The duct can be easily modified with screens and other flow modifying devices upstream of the probe. A perforated plate is used in the experimental tests to carry out “sensitivity” investigations of the probe tip heat transfer coefficient to a change in the turbulence level of the flow upstream of the probe tip. The flow temperature is measured downstream of the flow smoothing screens approximately 6 inches upstream of the probe station. A photograph of the test apparatus is shown in Figure 2.

Dry pressurized air is used at the supply total temperature which is thermally stabilized by flowing through approximatly1100 ft. of buried pipe. The air flow is regulated to produce a duct mass flow of 1 to 4 lbm/s measured by a FlowDyne® Venturi Flowmeter PN:VPO41563-SF.

The duct is open to the atmosphere, and duct pressures are slightly above the atmospheric pressure of ~14.2 psia at the test location. The UTSI high pressure air storage facility will hold about 13000 lbm of air at a tank pressure of 3000 psig.

Excessive cooling of the high pressure regulator limits the minimum tank pressure to approximatly1500 psig, giving about an hour of testing before recharging the tank, depending on the required flow rates. The pressure is regulated to 80 to 100 psig by the high pressure regulator and further reduced by a valve at the test cell. This valve may be set manually but does not have any control function, so any failure of the high pressure valve to control precisely is seen at the test cell as a variation in the pressure and the mass flow rate. The air temperature varied from 25 to 30°C during the course of the testing and drifted no more than 1°C during any test point.

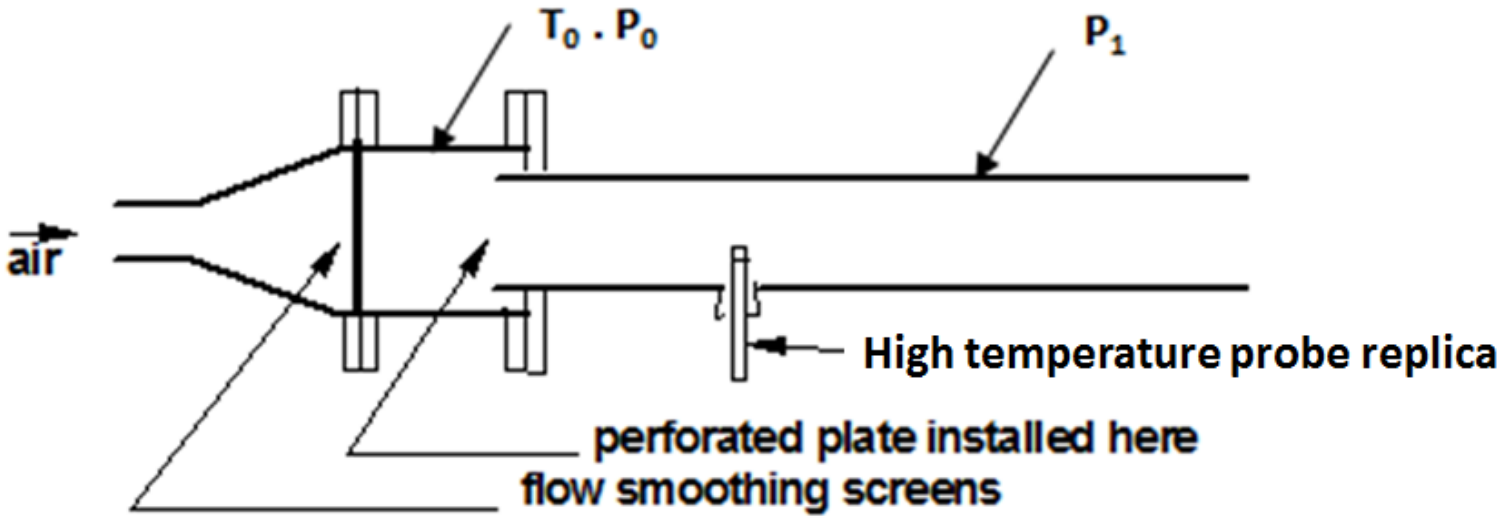

Figure 1: Schematic Drawing of the Test Apparatus.

Figure 2: Photograph of the Facility Test Section Attached to the Stilling Chamber (plenum) in the UTSI Propulsion Research Facility.

2.2 INSTRUMENTATION

2.2.1 PROBE

The test article consists of a heated probe that is instrumented with thermocouples. The probe tip is fabricated using aluminum and is attached to a stainless steel support tube. The probe tip has a diameter of 1 inch and a length of 1.25 inches. The tip is drilled to accept a 0.375 inch diameter cartridge heater with graphite impregnated walls (Omega PN: CSH-201100/120). Thermally conducting grease is used to minimize the contact resistance between the cartridge heater and the aluminum tip. Omega model KMQXL-062G-12 type K thermocouples are installed in 0.0625 inch holes drilled to various depths relative to the surface of the tip. These embedded thermocouples provide an average temperature and are used to detect thermal gradients in the probe. There is also a similar thermocouple centrally installed above the cartridge heater to monitor for radial temperature gradients. Polyurethane foam is used as a thermal barrier to attach the aluminum probe tip to the stainless steel support tube. The foam fills the approximately 1/8 inch gap between the tip and support tube. The foam is reinforced by the 0.0625 inch thermocouples and the heater leads. An illustration of the probe configuration is shown in the Figure 3.

The polyurethane foam provides structural support and thermal isolation/insulation of the aluminum probe tip from the stainless steel support tube. In order to ensure that the foam would perform as desired, a number of tests were performed to examine its relevant properties. These tests are described below.

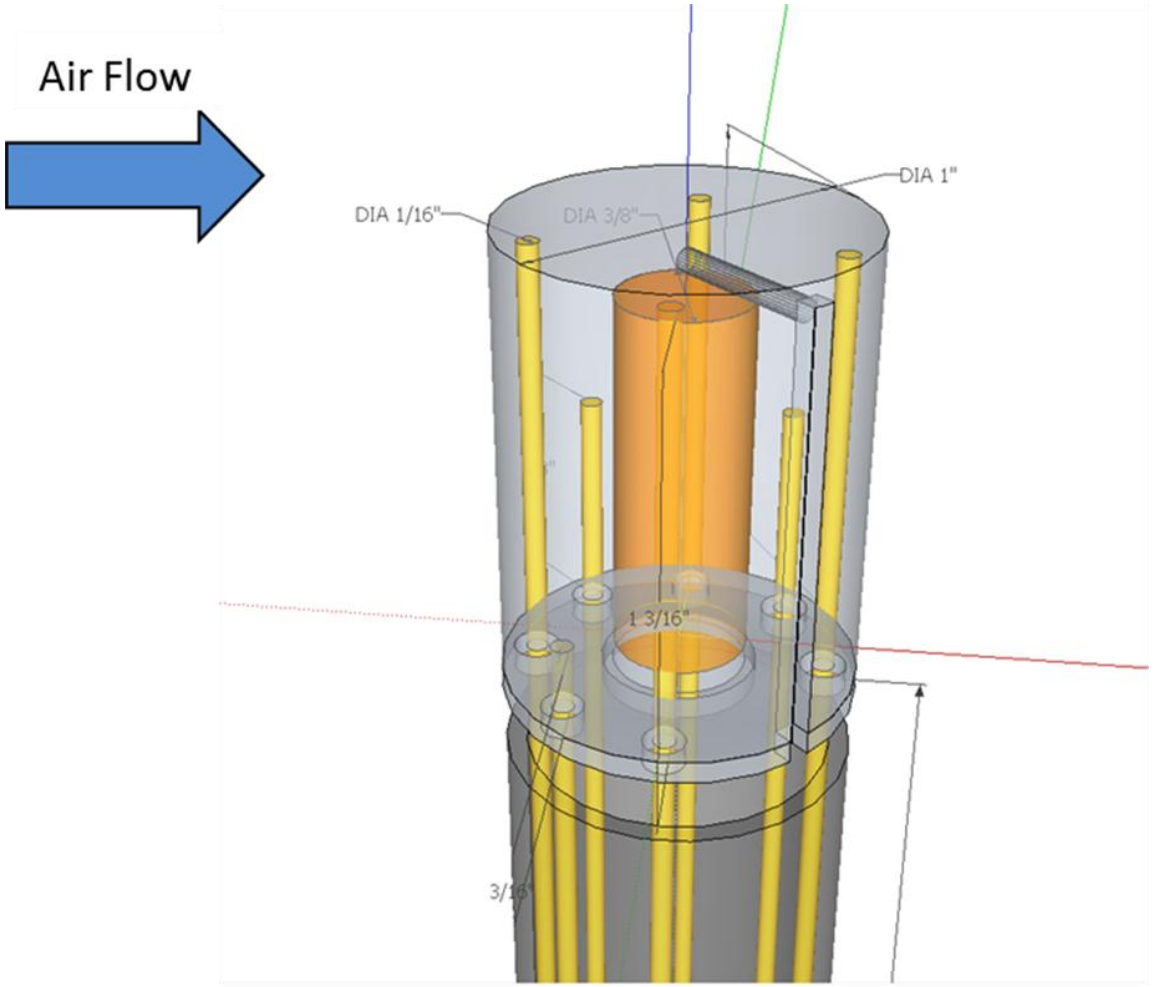

Figure 3: Schematic of the Assembled Simulated Temperature Probe.

2.2.2 TEMPERATURE

A cured piece of foam, approximately 3 inches by 1 inch in length, was placed in an oven at temperatures up to and exceeding those expected to be encountered in probe testing. The foam was exposed to temperatures of 100°C and 110°C for 30 minutes with no change in properties. The oven temperature was then increased to 125°C, and the foam was again set in the oven for 30 minutes. This resulted in a slight darkening of the foam, but no change in stiffness. Finally, the foam was left in the oven for 10 minutes at 140°C, and although there was increased discoloration, its consistency was again unchanged. These tests are a qualitative indication that the foam is stable over the range of expected temperatures.

2.2.3 RELEASE

The outer surface of the foam must maintain a smooth, one-inch diameter. A release agent (Synlube® 1711) was sprayed onto three different surfaces to examine whether the foam, after curing, would release from a mold. The surfaces tested were a shallow plastic dish, a plastic tube approximately 1 inch in diameter and 4 inches long, and a small metal container roughly two inches deep and two inches in diameter. After allowing the foam to cure for 24 hours, an attempt was made to slide the cured foam out of each of these objects. This test was a success. All three of the foam pieces released instantly with very little effort.

2.2.4 CURING

In order to determine how well spray foam would cure in an enclosed area such as a pipe, the foam was sprayed into several objects which would limit exposure to open air. The foam cured no more than 1.5 inches to 2 inches deep. The air curing spray foam was replaced by casting foam that was mixed with a catalyst before pouring into the probe support tube. This produced a solid block of foam. This material was used in the final test probe assembly. A photograph of the assembled simulated temperature probe is shown in Figure 4.

Figure 4: Photograph of the Assembled Simulated Temperature Probe.

2.3 TEST DESCRIPTION

The heat transfer coefficient (*h*) is defined in this work as:

$$h = \frac{(EI - q - C\frac{dT}{dt})}{A(T - T_0)} \qquad \text{Equation 2-1}$$

where *EI* is the electrical power to the probe heater, *q* is the heat loss from the system (including conduction in the heater leads and the thermocouples, and radiation from the probe surface). *A* is the probe tip surface area exposed to the flowing gas at temperature T_o, *T* is the probe temperature, and *CdT/dt* is the power storage associated with a change of temperature of the probe body. In this equation, a lumped mass assumption has been made. With the multiple thermocouples in the probe it is possible to make a qualitative assessment of the assumption of a bulk probe temperature and the lumped mass assumption.

2.3.1 PRETEST EVALUATIONS

Prior to the start of testing with air flow, two tests were made, one on the cartridge heater and one on the assembled probe. In the former, the heater was insulated with foam and pulsed with a known amount of power, while temperature data from a thermocouple mounted on the heater surface was recorded. The temperature time history was analyzed to determine the thermal capacity of the heater.

A similar test of the assembled probe enabled the evaluation of the overall thermal capacity of the assembly, as well as the heat loss by conduction through the heater leads and the thermocouples.

In addition, total pressure traverses were made at the probe location. The purpose of these tests is to document the test conditions and to establish the thickness of the

boundary layer for probe tests at different penetration depths. Traverses with a hot wire probe also were made to characterize the turbulence level. The total pressure probe and hot wire traverse were repeated with the turbulence modifying plate installed on the duct inlet. The information obtained in these tests helps quantify the sensitivity of the heat transfer coefficient correlation to the duct boundary layer properties and the flow turbulence.

2.4 TESTING

The items recorded by the data system are listed in Table 1. Those marked with an “h” in column “data reduction” are used in the calculation of the heat transfer coefficient (h) and the Reynolds number (Re), “t” indicates use in the total pressure traverse, and “q” in the insulated probe pretests. In all cases the duct static pressure was less than 0.1 psi above the ambient pressure, and the nominal atmospheric pressure (14.2 psia) was used for the duct static pressure. Details of the instrumentation and data acquisition system are provided in Appendix A.

Table 1: Parameters Recorded by the Data System.

Column	Item	Data Reduction	Notes
1	Seconds		
2	Venturi_Inlet_Pressure_(psig)		
3	Venturi_Differential_Pressure_(psid)		
4	DUT_Inlet_Pressure_(psig)		
5	Static_Pressure_1_(psid)		
6	Traversing_Total_Pressure_(psid)	t	Traverses or optional duct static
7	Plenum_Total_Pressure(psid)	t	
8	Venturi_Inlet_Temperature_(°F)		
9	Air_Heater_Output_Temperature_(°F)		
10	Probe_1_Temperature_(°C)	q,h	10-17 averaged to get T_{probe}
11	Probe_2_Temperature_(°C)	q,h	
12	Probe_3_Temperature_(°C)	q,h	
13	Probe_4_Temperature_(°C)	q,h	
14	Probe_5_Temperature_(°C)	q,h	
15	Probe_6_Temperature_(°C)	q,h	
16	Probe_7_Temperature_(°C)	q,h	
17	Probe_8_Temperature_(°C)	q,h	
18	Plenum_Chamber_Temperature_(°C)	h	Used for T0
19	Probe_Surface_TC	q,h	Insulated probe and duct wall
20	Heater_Voltage_(V)		Used to calculate Probe_Power
21	Heater_Current_(A)		Used to calculate Probe_Power
22	Control_Valve_Setting_(%_open)		
23	Dump_Valve_Setting_(%_open)		
24	Mass_Flow_(lbm/s)	t,h	Calculated from 2, 3, and 8
25	Probe_Depth_(in)	t	Used during traverses
26	Probe_Heater_On_(100_if_true)		
27	Probe_Power_(W)	q,h	

2.4.1 VELOCITY PROFILE

Total pressure traverses at the axial position in the duct where the temperature probe was tested were made both with and without a perforated plate installed (see in Figure 5). The probe was moved in steps, and the position was measured with a micrometer with a precision of 0.01 in. Total pressure was measured continuously, so some of the vertical scatter in the data shown in Figure 5 results from the radial motion of the probe between data points. The profiles without the perforated plate were taken from the centerline toward the wall, and the higher points at each location are most representative of the pressure at the indicated position. The profiles with the perforated plate were taken in the opposite direction and the most representative points are the lower values at the indicated position. These data are normalized by the value of plenum total pressure taken at the same time multiplied by the average plenum total pressure during the time of the traverse. The lines marked with the mass flow represent the values of P_t-P computed from the mass flow using the relationship:

$$V = \frac{M}{(\rho A)} \qquad \text{Equation 2.2}$$

$$\frac{P}{P_t} = \left[1 + \frac{(\gamma-1)}{2}\left(\frac{V}{a_t}\right)^2\right]^{\frac{\gamma}{(\gamma-1)}} \qquad \text{Equation 2.3}$$

$$P_t - P = \left(\frac{P_t}{P} - 1\right)P \qquad \text{Equation 2.4}$$

where a_t is the speed of sound at the total temperature, M is the average mass flow during the traverse, ρ= 0.070 lb/ft^3 at 25 °C and 1000 ft altitude and 50% relative humidity, A = 0.200 ft^2, γ = 1.4, and P = 14.2 lbf/in^2 (Anderson, 2003). There is little difference between these profiles, except for an indication that the velocity does not fall as fast near the wall when the perforated plate is installed. Both profiles are indicative of a developing flow.

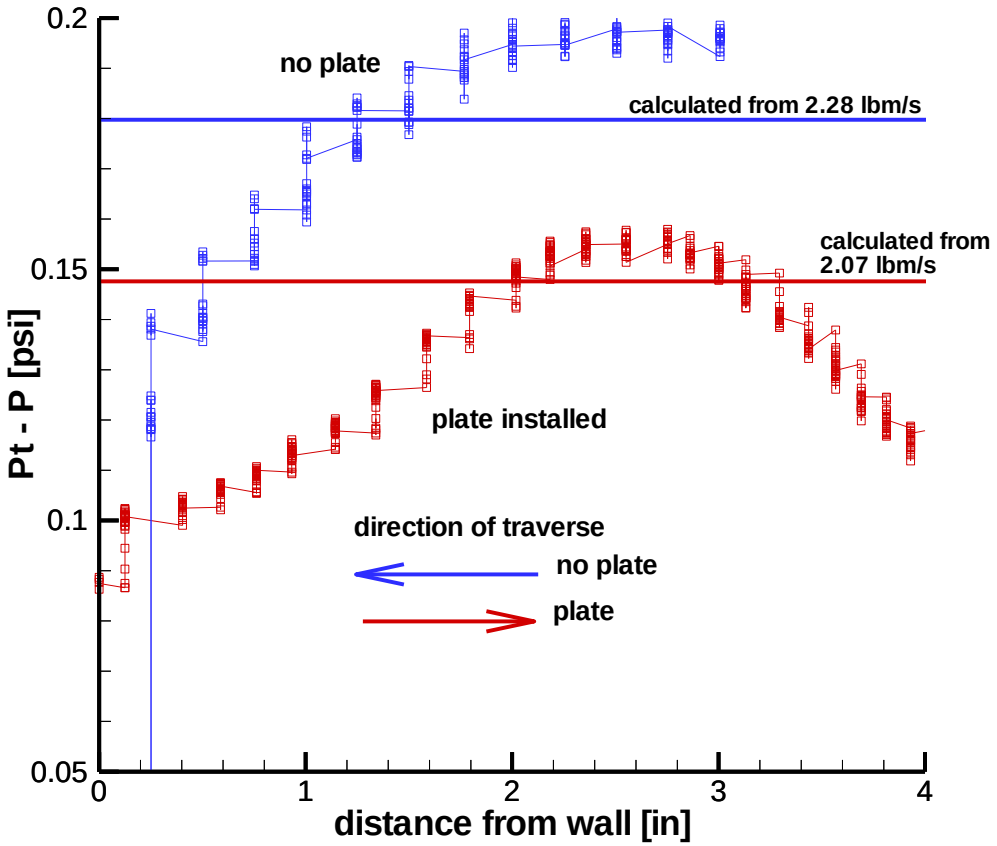

Figure 5: Total Pressure Profiles at Location of Simulated Temperature Probe.

3 TEST RESULTS

3.1 HEAT TRANSFER

The energy conservation equation for a body, consisting of a heater in a shell, intended to measure the bulk heat transfer coefficient is for the shell:

$$\rho V C_p \frac{dT}{dt} = hA(T_0 - T) + kA_h(T_h - T) - q_r - q_c \qquad \text{Equation 3.1}$$

and for the heater:

$$\rho_h V_h C_{ph} \frac{dT_h}{dt} = kA_h(T - T_h) + EI - q_{ch} \qquad \text{Equation 3.2}$$

Where (A) and (A_h) are the areas for the shell and heater respectfully. Also (T_0) and (T) are the probe temperature and the air temperature respectfully. Adding equations 3.1 and 3.2 eliminates the unmeasured heater temperature (T_h) and the effective conductivity (k) of the interface between the heater and the shell. At long times under steady conditions the transient terms both approach zero. At times where *dT/dt* is small, the sum of the transient terms may be approximated by *C dT/dt*. Here *C* is assumed to be a constant approximately equal to ($\rho V Cp + \rho_h V_h Cp_h$), where the subscript *h* denotes values for the heater. The value of *C* is chosen to minimize the variation in *h* over the final 200 to 300 seconds of the test point. The electric power to the heater is the product of the DC current (I) and the voltage (E), and is calculated by the data system. The conduction losses (q_c and q_{ch}) are lumped into one experimental value. The radiation loss (q_r) is calculated from:

$$q_r = \sigma \varepsilon A\left(T^4 - {T_w}^4\right)$$ Equation 3.3

The resultant equation for h is:

$$h = \frac{\left(EI - C\frac{dT}{dt} - q_r - q_c\right)}{\left(A(T - T_0)\right)}$$ Equation 3.4

The probe tip Reynolds number, based on the measurements made, is:

$$Re_d = \frac{m}{A_d}\frac{d_p}{\mu}$$ Equation 3.5

The mass flow rate (*m*) is a measured quantity, the viscosity (μ) is obtained as a function of temperature from the Sutherland equation (Sutherland, 1893), the duct area (A_d = 0.0186 m^2) and the probe diameter (d_p = 0.0254 m) are both constants for these tests.

The data required to evaluate the heat transfer coefficient-Reynolds number relationship for the baseline test case (1.8 inch probe penetration depth) may be seen in Figure 6. During the first test sequence, four different mass flow rates were used, with the final flow rate being a repeat of the first. It turned out that the ability to control mass flow was less than ideal. There is no active control on the air-flow regulator at the measuring venture of the blow down facility, and the storage tank regulator drifts, leading to an output with a saw-tooth oscillation as slow as 2 cycles per minute. This pressure fluctuation results in a corresponding mass flow variation that also shows up to a lesser degree in the probe temperature and the gas temperature.

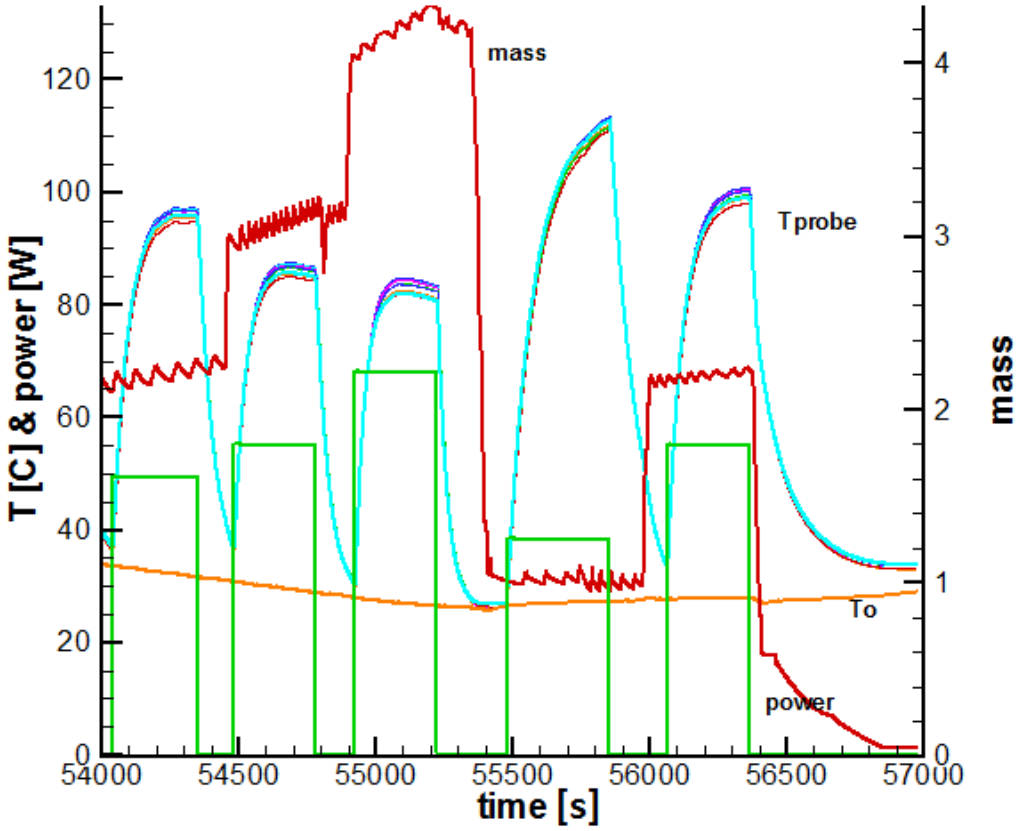

Figure 6: Raw Data from Test Sequence HeatedAirData 02-40-18PM of the Heated Simulated Temperature Probe in the Flow.

Data are recorded each second. They are the values of the variables averaged over the previous second by the data system. To obtain the most probable value of *h*, the average temperature of the probe is obtained from measurements corresponding to the eight thermocouples embedded in the probe. The average seems to be the best value to use to calculate *h*, since *h* is a bulk value based on a single probe temperature and the area of the un-insulated part of the probe. The heat transfer coefficient is calculated from the data at each second, filtered by selecting points where T_{avg}-T_o is greater than 20 °C and the heater is on. The heat transfer coefficient is then plotted against the Reynolds number, also calculated at each data point (Figure 7).

To evaluate the term *CdT/dt* in the equation for *h* (Equation 3.4) requires some judgment on the part of the data analyst. With the noise on the temperature data, the derivative term was averaged over a range of data points using the equation:

$$\frac{dT_i}{dt} = \frac{(T_{i+1} - T_{i-1})}{2}$$ (averaged over a series of consecutive time steps) Equation 3.6

where *i* is the index for the current time. The value of *C* that produced the least change in *h* with time for each run is 42 J/°C (Figure 8).

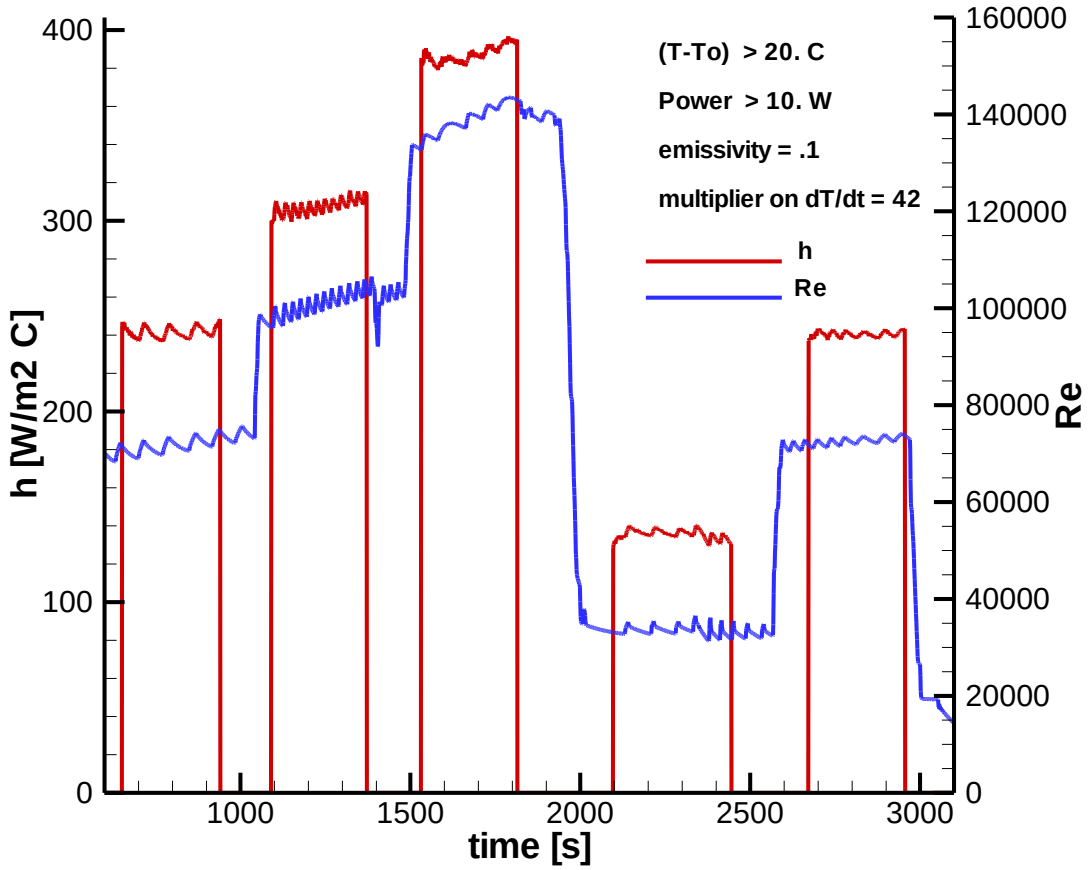

Figure 7: Convective Heat Transfer Coefficient and Reynolds Number for Each Second of the Run.

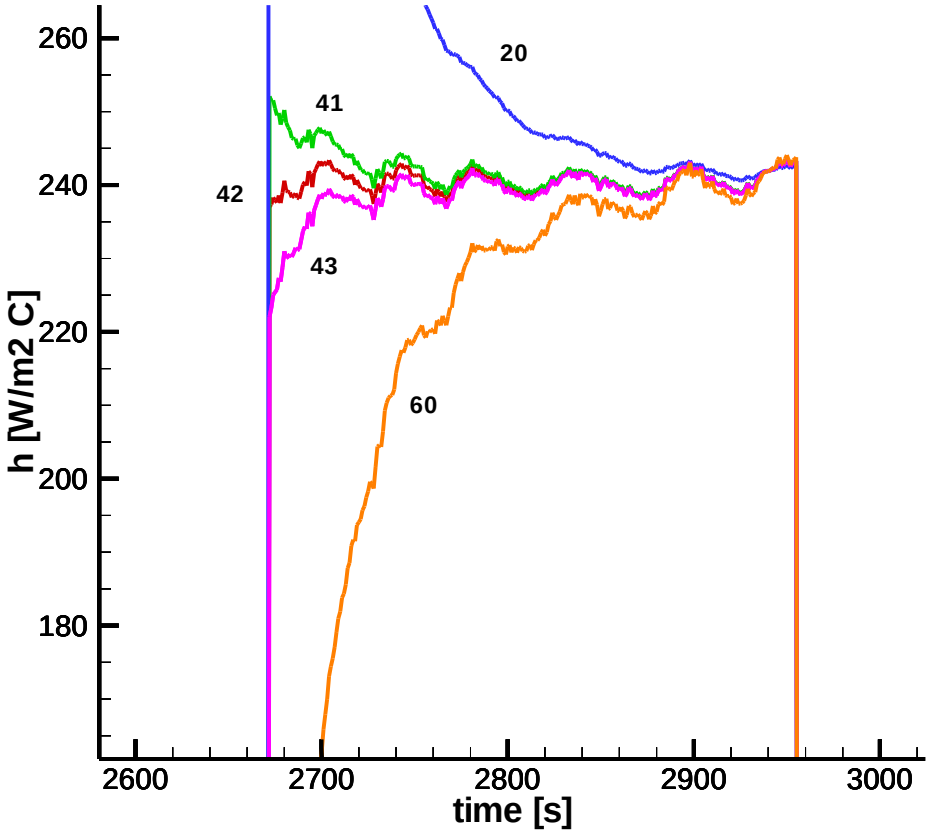

Figure 8: Variation of the Convective Heat Transfer Coefficient with the Parameter (C) in C dT/dt.

The radiation loss term (q_r) is evaluated from the equation for the radiant transfer for a convex body in a large cavity equation 3.3 (Bejan & Kraus, 2003):

$$q_r = \sigma A \varepsilon \left(T^4 - {T_w}^4 \right)$$

The parameters in the radiant transfer equation with the largest uncertainties are the emissivity (ε) of the aluminum probe body and the duct wall temperature T_w. The "Engineering Tool Box" (Engineering Toolbox) lists ε for commercial sheet and mildly oxidized aluminum at 0.09 and 0.11, respectively. A relatively small uncertainty in wall temperature can give a fairly large uncertainty in q_r. For example with a probe temperature of 77 °C (350 K), a 5 °C, uncertainty in T_w will give about a 10% uncertainty in q_r.

During the preliminary tests, the probe was tested where its tip was encased in a foam block to eliminate heat loss by convection and radiation. The heater in the probe was pulsed with current at different voltages and for different times to add a known amount of energy into the probe. The probe was then allowed to sit for approximately 10 minutes while the temperatures were recorded each second. The temperature drop during this time is attributed to conductive heat loss through both the heater electrical leads and the probe thermocouples. The probe specific energy calculated from the maximum temperature rise and the energy required to achieve it is listed in Table 2. It is expected that a significant fraction of the heat loss is by conduction through the copper leads of the heater and a lesser amount through the eight thermocouples, since the stainless steel sheaths and the chromel/alumel thermocouple wires are much poorer conductors. The heat loss is determined by the gradient where the leads attach to the heater cartridge. Using $k\,\Delta T/\Delta x$ implies a constant gradient in the wires, and even with copper it takes several minutes to approach this condition. This is shown in Figure 9 where the probe cooling rate divided by the temperature difference between the probe tip and the ambient temperature is shown as a function of time for six heating/cooling

cycles of the probe with an insulated tip. For the first 200 seconds of each cycle, the conductive heat loss decreases from about 40 mW per °C to about half of this as the gradient in the leads relaxes toward steady state. For the remainder of the cycle it averages about 21 $\pm$ 3 mW/ °C. Since the temperature of the probe (during heating) changes much more gradually when submerged in air flow than it does when the probe tip is insulated, it is assumed that the steady state value of 21 mW / °C is the appropriate value to use for these cases. The most critical test condition used 40 W to heat the probe to a ΔT of 85 °C. A 3 mW error in the estimate of heat loss would give about 0.25 W error, or about 0.6 % error, in the estimate of the heat transfer coefficient in this case, and less in the cases where more power was needed to achieve the same ΔT. When the parameters in Table 2 are applied to the complete data set, the individual realizations of *h* are shown along with the Reynolds number in Figure 7. It is interesting to note that the effect of fluctuations of Re caused by pressure variations seems to correlate quite well with the noise on *h* (Figure 6), which helps to explain the remarkably good correlation between *Re* and *h*.

Three test conditions were evaluated with the high temperature probe. The first of these was conducted with an immersion depth of 1.8 inches and an unobstructed inlet on the test duct. In the second test the end of the probe was moved to the six inch duct center line. The third test was a repeat of the first, with the turbulence augmenting plate (with 0.5-inch holes on 1.0 inch triangular centers) located at the inlet of the test section duct. The relationship between the heat transfer coefficient and Reynolds number changed only slightly for these configuration changes (Figure 10).

Table 2: Probe Specific Energy.

T_0°C	T_{max}°C	Energy J	J/°C
Insulated Probe Tip with Heater			
35.5	56.9	986.5	46.10
35.1	62.0	1229.2	45.70
35.1	67.8	1500.2	45.88
35.1	76.7	1797.1	43.20
35.3	111.7	3370.0	44.11
35.6	98.2	2759.0	44.07
26.0	89.2	2762.0	43.70
30.9	106.7	3371.0	44.47
27.6	69.5	1797.0	42.89
		Average	44.45
Insulated Heater Only			
28.8	54.3	167.0	6.55
27.3	115.7	499.0	5.64
20.9	72.7	334.0	6.45
32.8	80.6	334.0	6.99
33.5	85.2	334.0	6.46
		Average	6.42

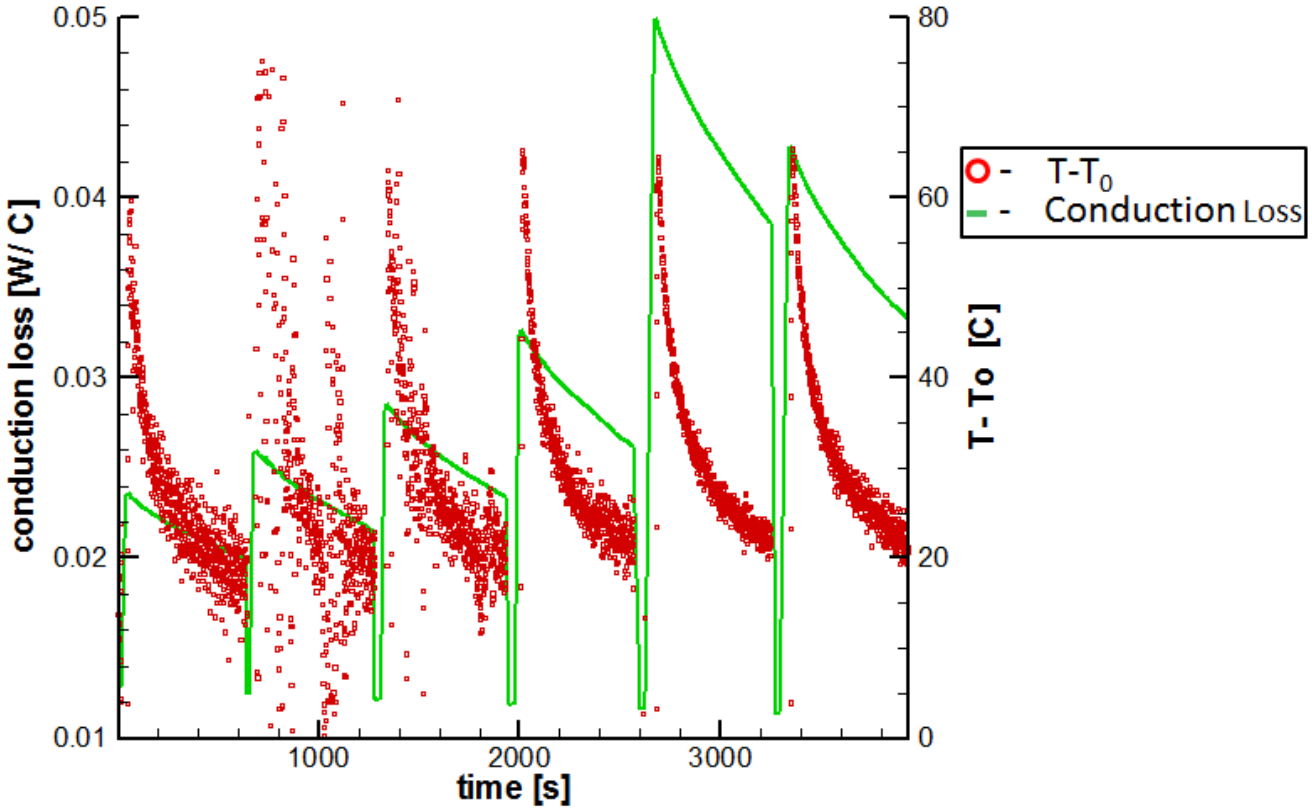

Figure 9: Insulated Probe Cooling Showing Temperature and Power Loss.

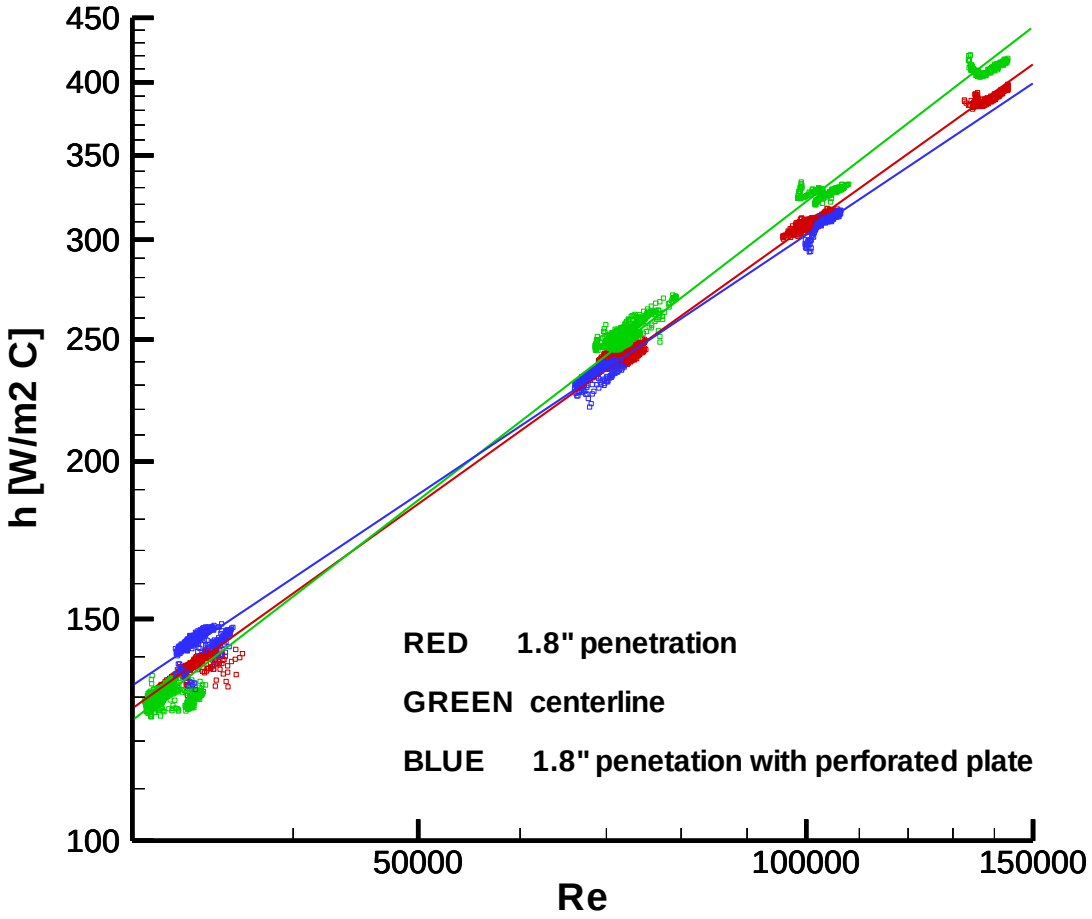

Figure 10: Convective Heat Transfer Coefficient Calculated from Measured Data from Airflow at 298K nominal.

These data from the three tests show a fair amount of scatter. Much of this is caused by the fluctuations in the inlet pressure and the resulting fluctuations in mass flow. There is a tendency for the higher mass flows (and thus higher Reynolds numbers) to give higher heat transfer, but this compensation is not perfect because of the finite time required to change the probe temperature.

Each of these data sets was fitted to a straight line on the log-log plot giving a function of the form:

$$h = aRe^n \qquad \text{Equation 3.7}$$

The coefficients *a* and *n* are listed in Table 3. The best fit lines for each of these data sets are included in Figure 10. The run with the probe at the centerline has a greater slope than that of the baseline case, and the baseline case has a best fit line with a slightly steeper slope than that for the with the perforated plate. The uncertainties associated with this data are described in detail in a later section.

The test 1 data set contains three separate runs at different final probe temperatures at a Re of about 72,000 (Figure 11). This is an enlargement of a section of Figure 7 showing typical data from three separate test points of Run 1 distinguished by the power applied to the probe and the resulting temperature rise. The scatter in the averages of the individual points is probably a result of the pressure fluctuation induced noise and does not reflect any dependence on temperature.

Table 3: Coefficients of $\boldsymbol{h = aRe^n}$.

Test / Color	a	n	σ (one std. dev.)
1 / Red	0.0672	0.732	1.01%
2 / Green	0.0381	0.785	1.02%
3 / Blue	0.115	0.684	1.01%

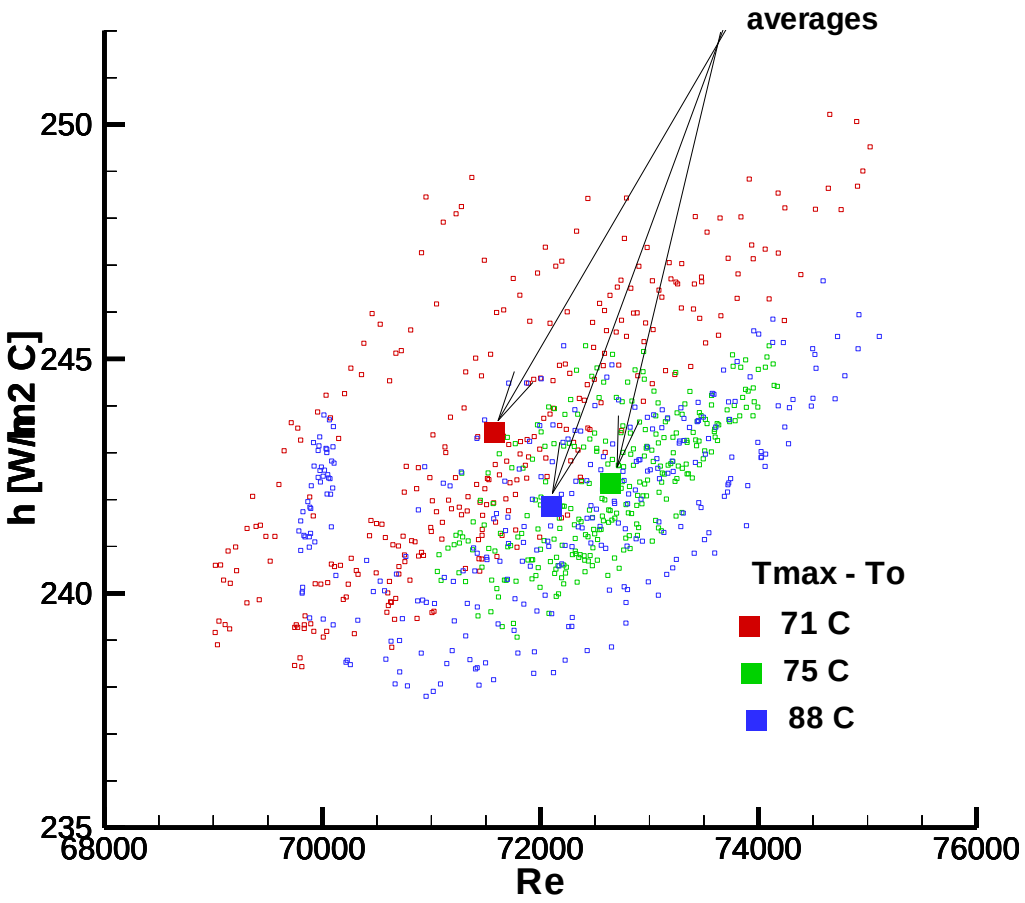

Figure 11: Effect of Temperature on the Heat Transfer Coefficient.

3.2 TEMPERATURE VARIATION

This discussion attempts to resolve the cause of the variation in temperature of the eight thermocouples in the probe. The extent of this variation is shown in Figure 12, where the reading at each one second data point for each thermocouple is averaged for each run consisting of 3 to 5 test conditions. Five of these measurements are made within 0.1” of the top surface of the probe, two near the middle, and one near the insulator separating the 1.25” long cylindrical probe tip from its support (Figure 13). In addition the probe was rotated 90 degrees in the run with the probe tip on the duct centerline, moving the leading edge from TC4 to TC6. This reversed the positions of TC3 from the leading to trailing quadrant and TC7 from the trailing to leading quadrant. None of the data in the figure shows any systematic variation which can be explained by either the position of the thermocouple on the probe or the orientation of the probe to the air flow. These data are too consistent to be random errors which leaves the most probable cause to be a deviation of the slope of the individual thermocouple calibration curves from the ideal curve for a type K thermocouple used by the data acquisition system.

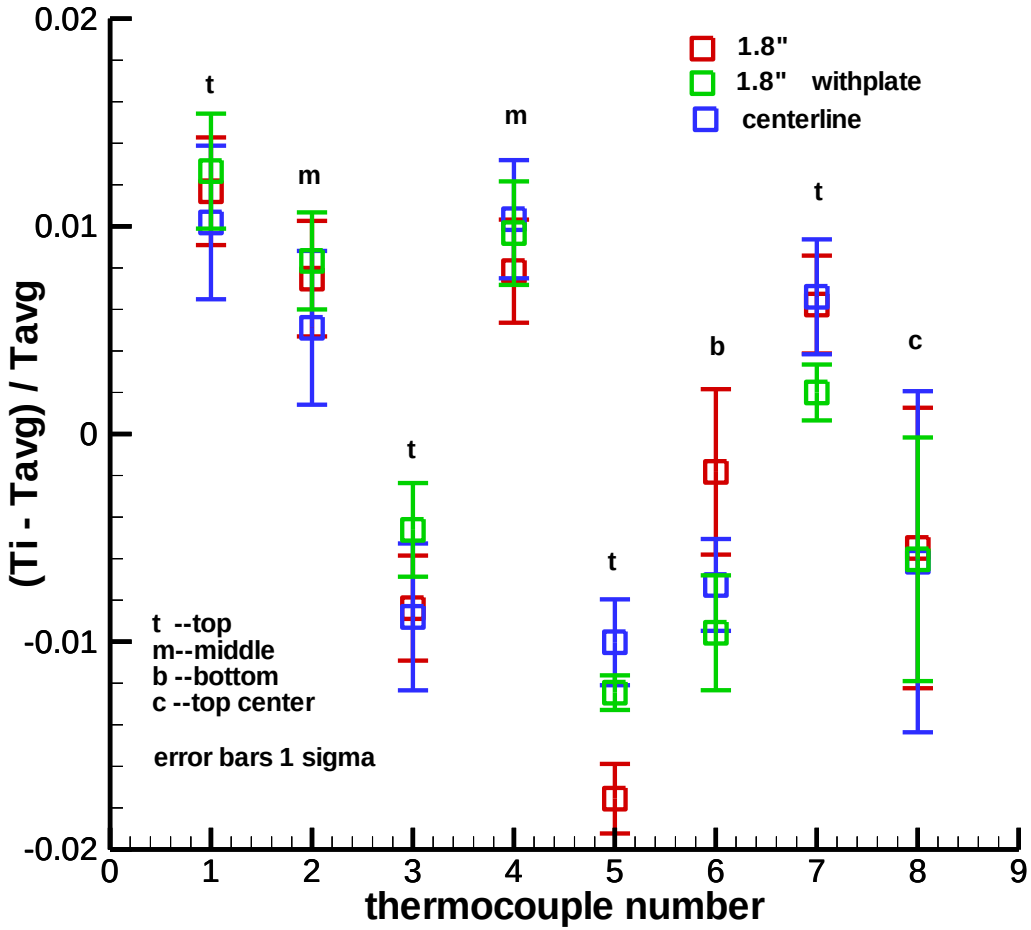

Figure 12: Probe Temperature Scatter.

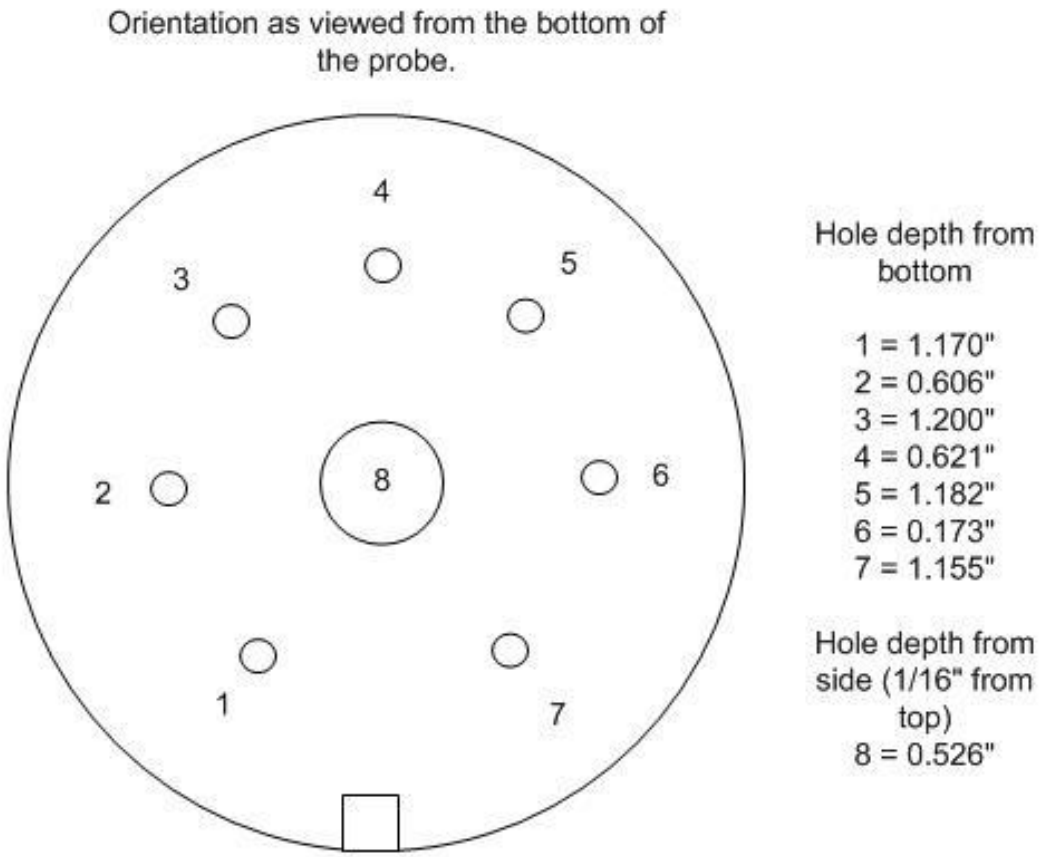

Figure 13: Schematic Showing Location of Thermocouples Embedded in the Probe.

3.3 NUSSELT NUMBER CORRELATION

A least square fit of all of the heat transfer data from the three test conditions (Figure 10) results in the heat transfer / Reynolds number (Re) relationship for 30000 < Re < 150000:

$$h = 0.060Re^{0.743} \text{ with } \sigma = 2.7\% \qquad \text{Equation 3.8}$$

All of this data was taken on a 0.0254 m (1 in) diameter probe in 25 °C air with a thermal conductivity (*k*) of 0.024 W/m°C and a Prandtl number (*Pr*) of 0.71. With the assumption that the Nusselt number will fit the functional form $Nu = a\,Re^{n}\,Pr^{1/3}$, the relation for *Nu* becomes:

$$Nu = \frac{hD}{k} = 0.071Re^{0.743}Pr^{\frac{1}{3}} \qquad \text{Equation 3.9}$$

for 30,000 < Re < 150,000.

The individual calculations are shown with the 1.8” penetration in red, the centerline location in green, and the runs with the turbulence augmenting plate in blue (Figure 14). The higher turbulence data (green) might suggest a slightly steeper slope; however, as will be seen later, these data are close to being within the uncertainty of the data from the run without the perforated plate.

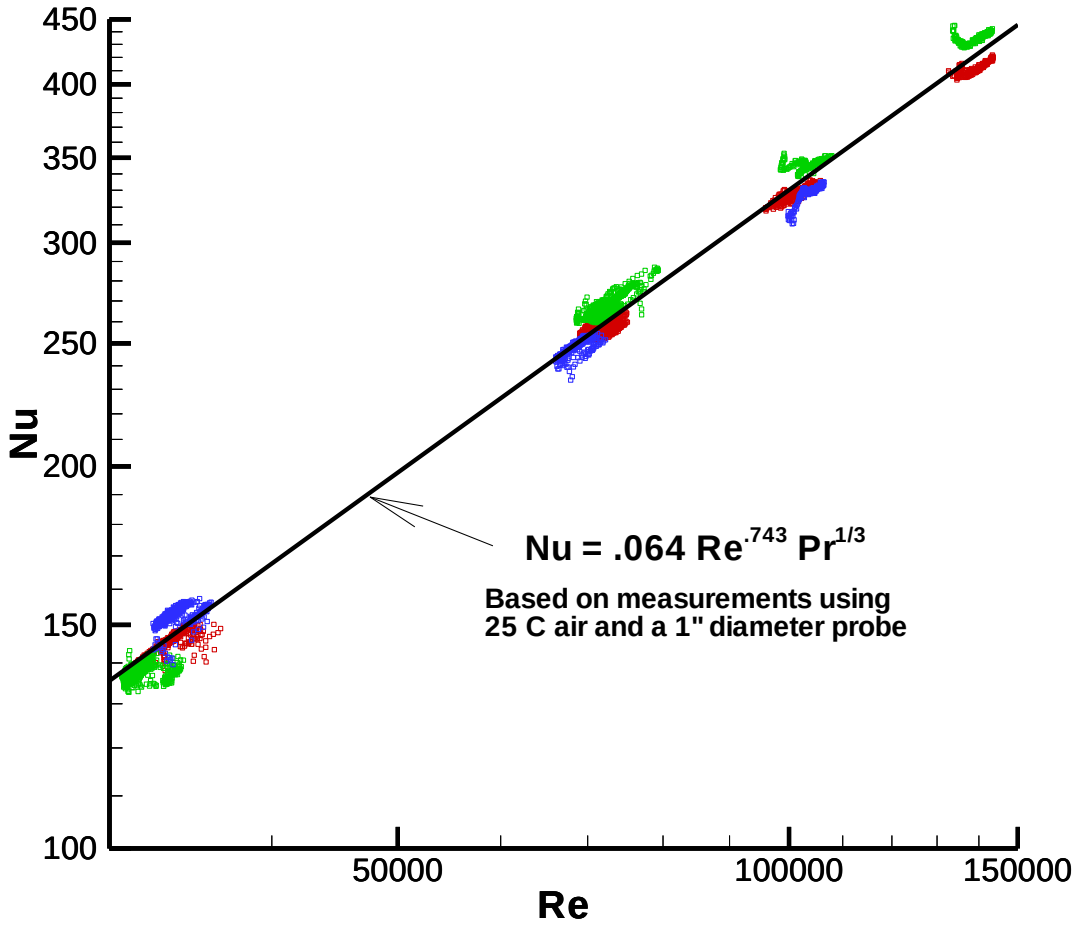

Figure 14: Nussult Number Relationship for the High Temperature Simulated Temperature Probe.

3.4 TURBULENCE EFFECTS

One of the requirements of these tests is to determine the effect of turbulence level on the heat transfer coefficient. For one series of tests a 1/8” thick aluminum plate with ½” holes on 1” equilateral triangular centers was attached to the inlet of the 6” test section duct. This produced parallel jets that had approximately three core lengths to mix before reaching the probe measurement station. Hot wire measurements both three inches upstream and three inches downstream of the probe show that the plate significantly increases the turbulence level at all scales.

Measurements of velocity and turbulence level were made in the test duct with a TSI Inc IFA 300 Thermal Anemometer System (with a TSI Model 1201-20 thin film sensor). The velocity data was sampled at 10,000 Hz for a total of 132,000 points for each of three radial positions at two axial positions (6 in. upstream and 6 in. downstream of the simulated temperature probe) both with and without the perforated plate installed. The data were reduced by the hot wire system into the average velocity during the sampling period, the turbulence level, and several other statistical quantities (Table 4 shows typical data for one test condition).

Table 4: Thermal Anemometer System Statistics – Upstream – Centerline – With Plate.

Measurement	Value
Mean Velocity	140.0
Normal Stress	127.1
Standard Deviation	11.3
Turbulent Intensity	-8.9%
Skewness	-0.75
Kertosis	4.33

Measurements were made 6 in. upstream and 6 in. downstream of the probe axial position in the duct. The mean velocity is normalized by the velocity calculated from the mass flow by the formula $V_{normal} = V_{hotwire} * V_{mass\ flow} / V_{mass\ flow\ 1}$ where $V_{mass\ flow\ 1}$ is the bulk velocity calculated from mass flow when the hot wire probe was on the centerline in the upstream position. This was done in an attempt to correct for the changes in flow velocity caused by the failure of the high pressure regulator valve on the air tank farm to maintain a constant pressure. During these tests the mass flow varied between 2 and 2.3 lbm/s.

An attempt was made to correlate the hot wire record times with the time on the mass flow records but this could not be done exactly. For this reason and perhaps because of vagaries in the hot wire system, there is a lot of scatter in both the velocity (Figure 15) and turbulence level (Figure 16) data. The mean velocity at 1 in. from the wall in the forward position with the perforated plate installed is abnormally low, as is the turbulence level with the perforated plate in the aft position at the same radial station. No data was obtained with the plate in the downstream position 2 in. from the wall or downstream without the plate on the centerline. Unfortunately, by the time these anomalies were discovered it was too late to repeat the tests. In spite of these problems, the velocity data show a decrease from the centerline toward the wall with no significant difference between the cases with and without the perforated plate.

The turbulence is significantly higher with the plate installed, and for both cases increases toward the wall. The difference in turbulence level is also seen in the power spectral density upstream on the centerline (Figure 17) where the plate not only shows a higher intensity but also maintains it at higher frequencies. In spite of the significant difference in turbulence the relationship between the heat transfer coefficient and Reynolds number changed very little with turbulence level (Figure 10).

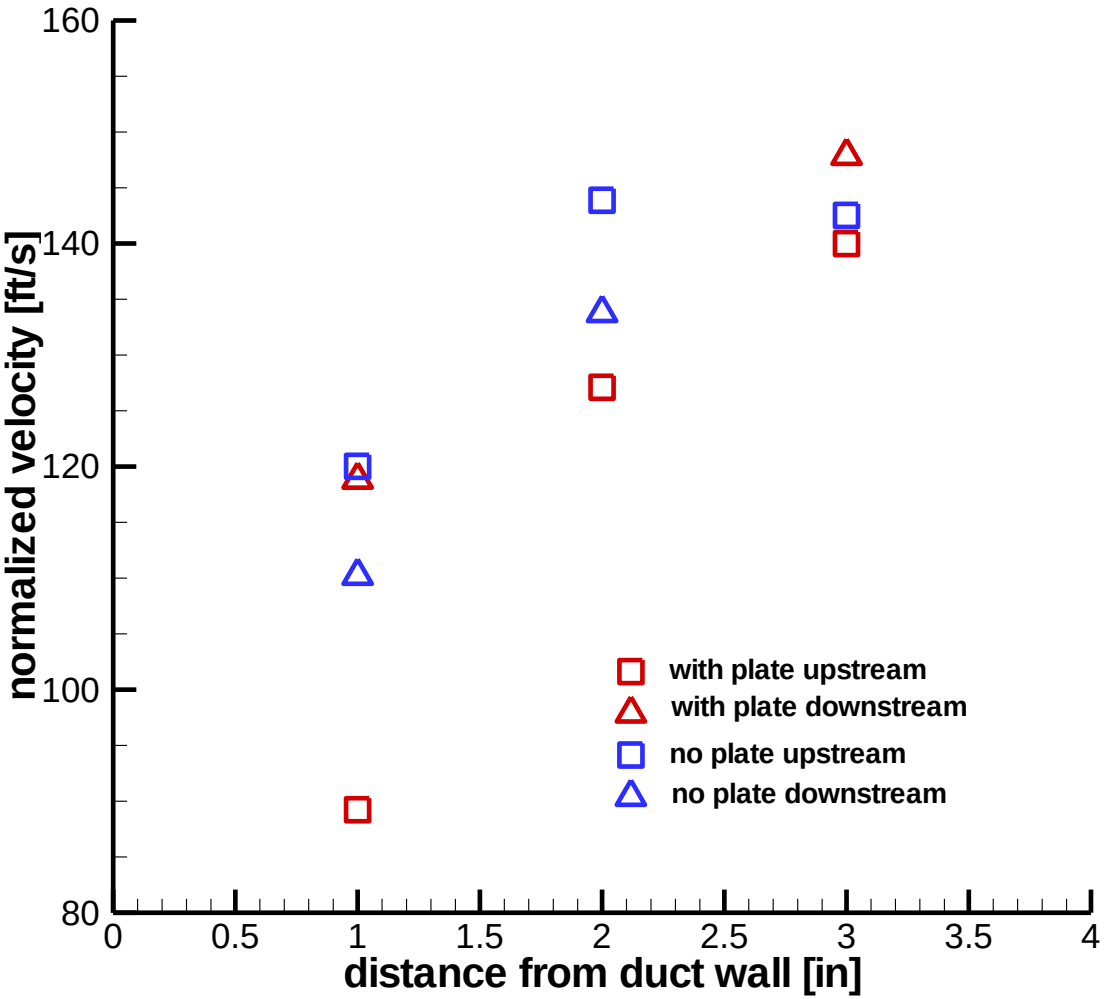

Figure 15: Velocities Measured Using Hot Wire Anemometer.

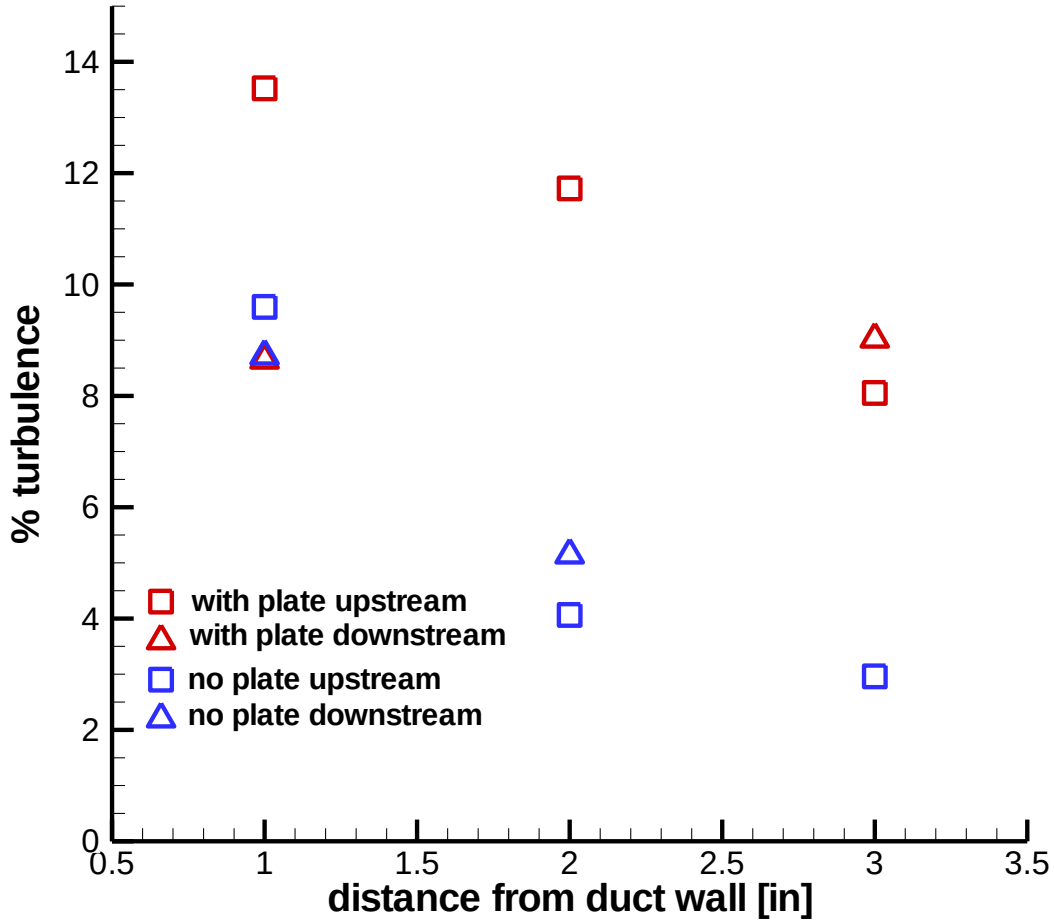

Figure 16: Relative Turbulence Levels Measured Using Hot Wire Anemometer.

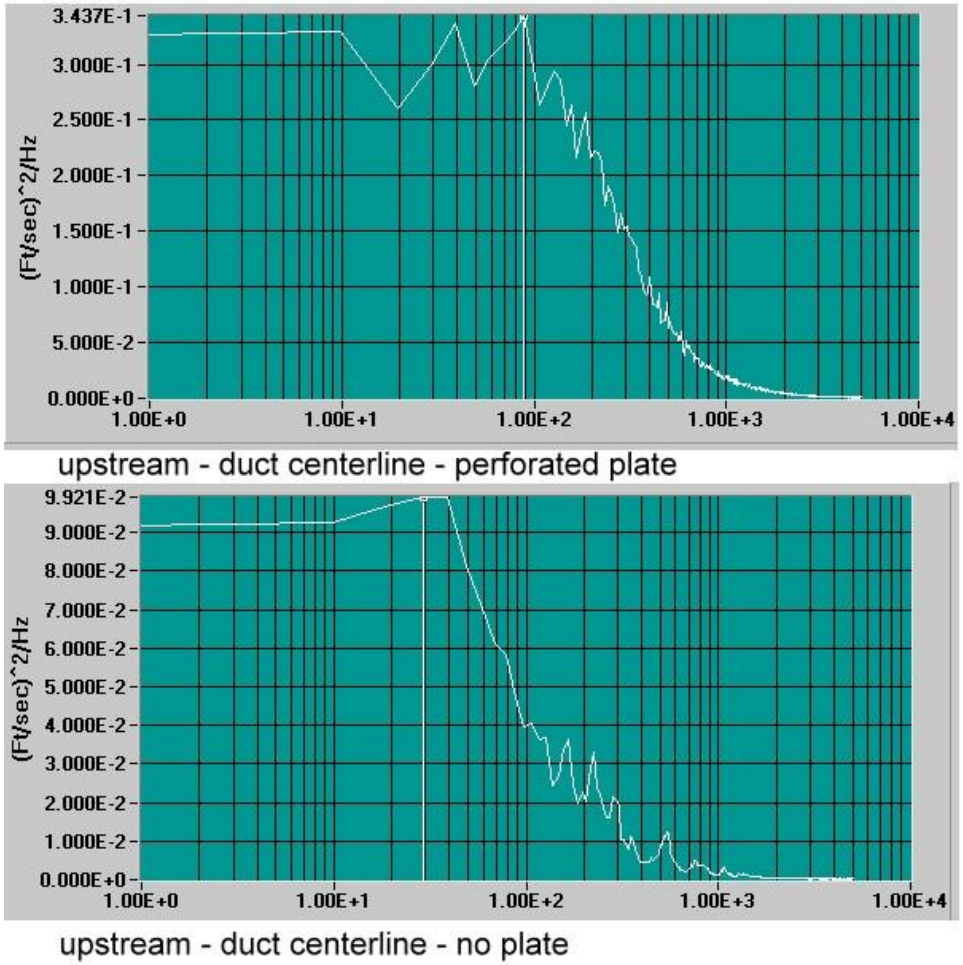

Figure 17: Power Spectral Density Upstream of the Centerline Measured Using Hot Wire Anemometer.

4 ERROR ANALYSIS

The general form for the uncertainty of a parameter (Y), which is a function of a number of variables (x), is:

$$Err(Y) = \left(\left(\sum \frac{\partial Y}{\partial x} err(x)\right)^2\right)^{\frac{1}{2}} \qquad \text{Equation 4.1}$$

where the error (Err) for a parameter (Y) is related to the errors (err) for a number of variables (x)The variables of interest here are the heat transfer coefficient (*h*), the Reynolds Number (*Re*), and the Prandtl Number (*Nu*). The equation for *h* used in this analysis is:

$$h = \frac{\left(EI - q_r - q_c - C\frac{dT}{dt}\right)}{\left(A(T - T_0)\right)} \qquad \text{Equation 4.2}$$

where

$$q_c = k(T - T_0), \qquad q_r = \sigma \varepsilon A\left(T^4 - {T_0}^4\right)$$

There are eight embedded thermocouple temperature measurements in the probe that are averaged to get the probe temperature (*T*).

$$T = \sum \frac{T_i}{n} \quad \text{and} \quad \frac{\partial T}{\partial T_i} = \frac{1}{n} \quad \text{so that} \quad \frac{\partial h}{\partial T_i} = \frac{\partial h}{\partial T}\frac{1}{n} \qquad \text{Equation 4.3}$$

The terms in the uncertainty equation are, assuming the uncertainty in all the T_i's are the same, $n(\partial h/\partial T_i \ err(T_i))^2$, which is equivalent to $n(\partial h/\partial T/n \ err(T_i))^2$. If the expression

$(\partial h/\partial T\ err(T))^2$ is used, then $err(T) = err(T_i)/\sqrt{n}$. The variables comprising *h* and the partial derivative are listed in Table 5.

Table 5: Components of the Uncertainty of *h.*

Variable	Symbol	Err (V)	$\partial h / \partial V$
Probe temperature	*T*	1/ √8 K	$(-4\ \sigma\varepsilon A\ T^3 - k) / (A\ (T-To)) - h / (T-To)$
Air temperature	*To*	1 K	$(4\sigma\varepsilon A\ To^3 + k) / (A\ (T-To)) + h / (T-To)$
Voltage	*E*	1%	$I / (A(T-To))$
Current	*I*	1%	$E /(A(T-To))$
Probe area	*A*	0.5%	$-qr/(A^2(T-To)) - h/A$
Probe emissivity	*E*	0.02	$-qr/(e\ A\ (T-To))$
Coefficient for *dT/dt*	*C*	0.5 J/K	$-(dT/dt)/(A\ (T-To))$
dT/dt	*Dt*	0.01 K/s	$-C /(A\ (T-To))$
Coefficient for q_c	*K*	0.03 W/K	$-1/A$

In Figure 18 the calculated values and the uncertainty of *h* (using equation 4.1) are shown plotted against time, indicating how the uncertainty varies as the probe temperature relaxes toward steady state. If one accepts the criteria that *h* calculated at long times (where *dT/dt* approaches zero) is the correct answer, the result that the same value of *h* is obtained at earlier times (with a non-zero *dT/dt*) indicates that the correction for a non-zero *dT/dt* works remarkably well. The criteria selected for data to be included in the data set is that both the power to the heater be on and the value of (T-To) be greater than 50 C. This can, in some cases, result in (*T-To*) nearly doubling between the start and end of the data collection for a test condition. This leads to a large change in the uncertainty of *h* over the same time, even though the value of *h* does not change appreciably. The average value and the standard deviation of *h* and *h_err* are shown for each test condition as a function of *Re* in Figure 19. The variation in *h* is caused principally by the inability of the probe temperature to follow exactly the fluctuations in mass flow and the noise introduced by the numerical derivative *dT/dt*. The relatively large standard deviation on the uncertainties is not random but rather results from the variation in the term over the sampling time.

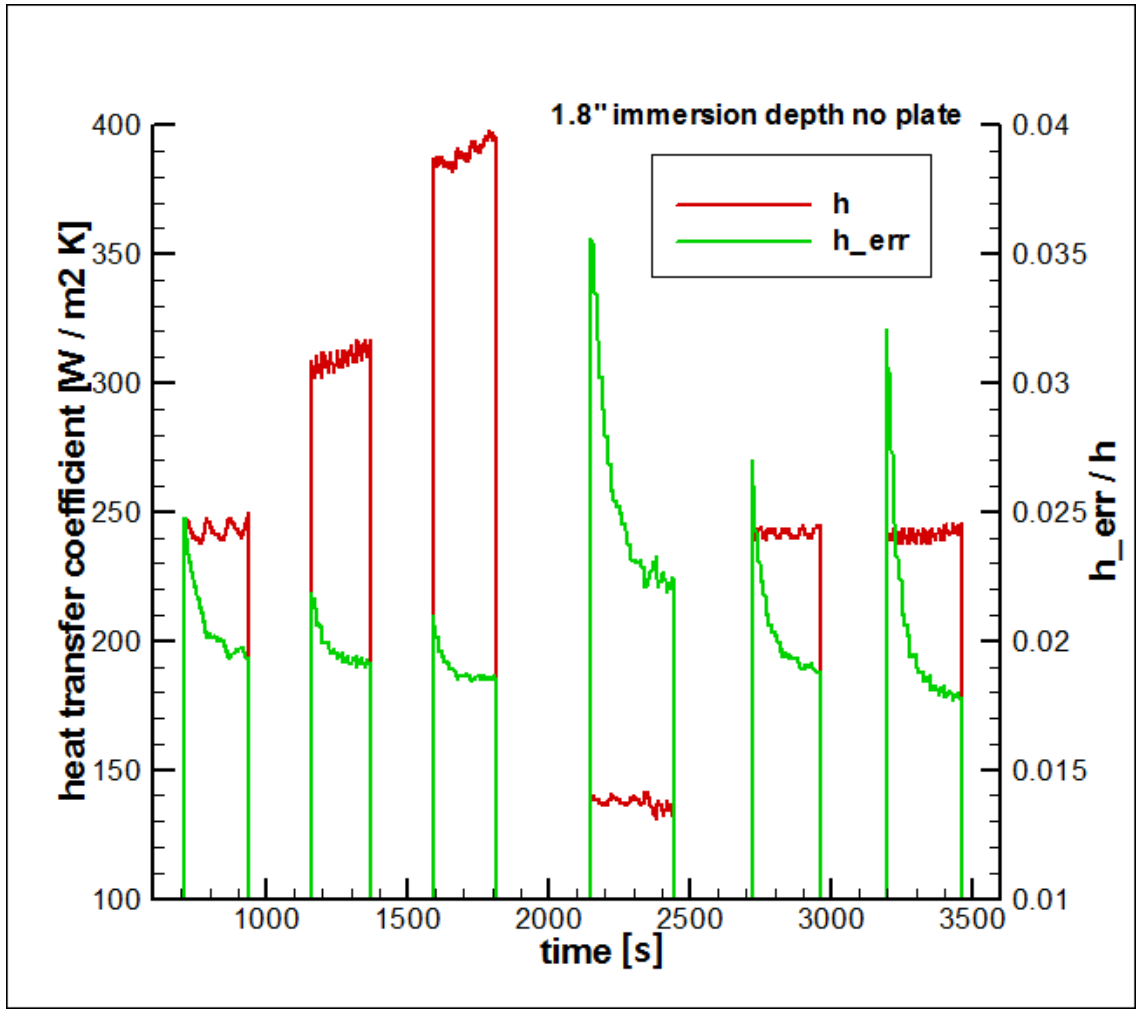

Figure 18: Heat Transfer Coefficient and Uncertainties for the Baseline Case.

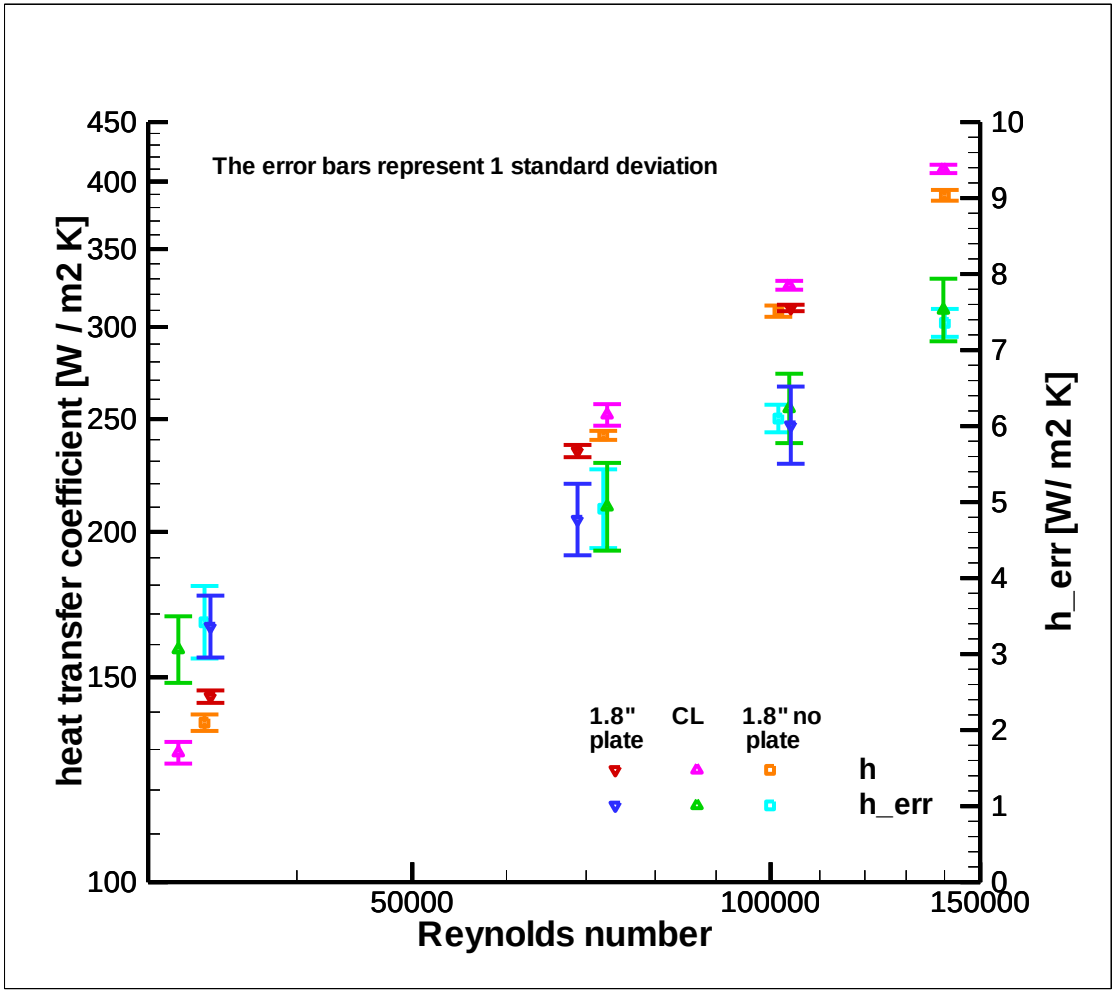

Figure 19: Heat transfer Coefficient and Uncertainties for all the Test Cases.

The equation for *Re* is:

$$Re = \frac{Gd}{u},\ G = \frac{m}{A_d},\ \text{and in a venturi,}\ \ m \sim \left(p\frac{\Delta p}{T_v}\right)^{\frac{1}{2}} \qquad \text{Equation 4.4}$$

The mass flow rate (*m*) is computed by the data system from the flow through the Flowdyne® venturi meter. For the purpose of computing the uncertainty, the equation for a venturi is used so that the uncertainty in the mass flow is a function of the venturi inlet pressure (*p*), the pressure drop from the inlet to the throat (Δp), the inlet temperature (T_v), and an intrinsic uncertainty in the meter (0.005**m*). The variables comprising *Re* and the partial derivatives are listed in Table 6, and the average Reynolds number, standard deviation, and uncertainty (calculated using equation 4.1) in Table 7. The uncertainty in the Reynolds number ranges from 1.22% to 1.24%.

In a similar fashion, the uncertainty associated with the Nusselt number can be calculated. The functional form of the Nusselt number introduced earlier is:

$$Nu = \frac{hD}{k} = 0.71Re^{0.743}Pr^{\frac{1}{3}} \qquad \text{Equation 4.5}$$

for 30,000 < Re < 150,000 and assuming that 1/3 is the correct exponent for Pr.

This Nusselt number correlation assumes the Prandtl number exponent is the same as that typical for cylinders in cross flow (Incropera & Dewitt, 1990). The variables comprising *Nu* and the partial derivatives are listed in Table 8. The Reynolds number and its uncertainty (1.23% typical) can be calculated as described above. The range of Prandtl numbers of the heated high pressure air to be used with the high temperature environments, calculated with the CEA code (Gordon & McBride, 1994), was found to be 0.7 to 0.75 inclusive. Assuming that the Prandtl number is known to within 0.01, the

corresponding uncertainty is 1.4%. Using these values in equation 4.1, the uncertainty of the Nusselt number is 1.86%.

Table 6: Components of the Uncertainty of Re.

Variable	Symbol	err	Partial of Re
Mass	m	0.5%	Re/m
Inlet pressure	p	1%	$0.5\ Re\ /\ p$
Pressure drop	Δp	1%	$0.5\ Re\ /\ \Delta p$
Inlet temperature	T_v	1 K	$-0.5\ Re\ /\ Tv$
Air temperature	T_o	1 K	$-5e\text{-}8\ Re/\mu$
Probe diameter	d	0.2%	Re/d
Duct area	A_d	0.5%	$-Re/A_d$

Table 7: Reynolds Number Scatter and Uncertainty.

Run	Re	σ/Re	Re_err/Re
1.8” no plate	3.35E+04	2.90E-02	1.23E-02
	7.24E+04	1.58E-02	1.23E-02
	1.02E+05	1.83E-02	1.23E-02
	1.40E+05	1.53E-02	1.24E-02
Centerline no plate	3.18E+04	2.55E-02	1.23E-02
	7.29E+04	2.61E-02	1.22E-02
	1.04E+05	1.53E-02	1.23E-02
	1.40E+05	1.48E-02	1.24E-02
1.8” with plate	3.38E+04	2.45E-02	1.23E-02
	6.88E+04	1.96E-02	1.22E-02
	1.04E+05	1.33E-02	1.24E-02

Table 8: Components of the Uncertainty of Nu.

Variable	Symbol	err	Partial of Nu
Reynolds Number	Re	1.23%	Nu/Re
Prandtl Number	Pr	1.4%	Nu/Pr

It should be noted that the data reduction shown in the section “Heat Transfer Results and Analysis” was done using a cut off $T-T_0$ of 20 ºC and the error analysis used 50ºC for the same parameter. This was done because the uncertainties at the start of a test became unrealistically large, considering the change in the predicted heat transfer coefficients (Figure 20). The green data points were reduced with a 20 ºC ΔT and are overlaid with the 50 ºC ΔT points in red, so that the points which are excluded by increasing the cutoff temperature are shown in green. It would be possible to repeat the data reduction at the higher cutoff temperature, but it was felt that the change would not be significant enough to justify the effort.

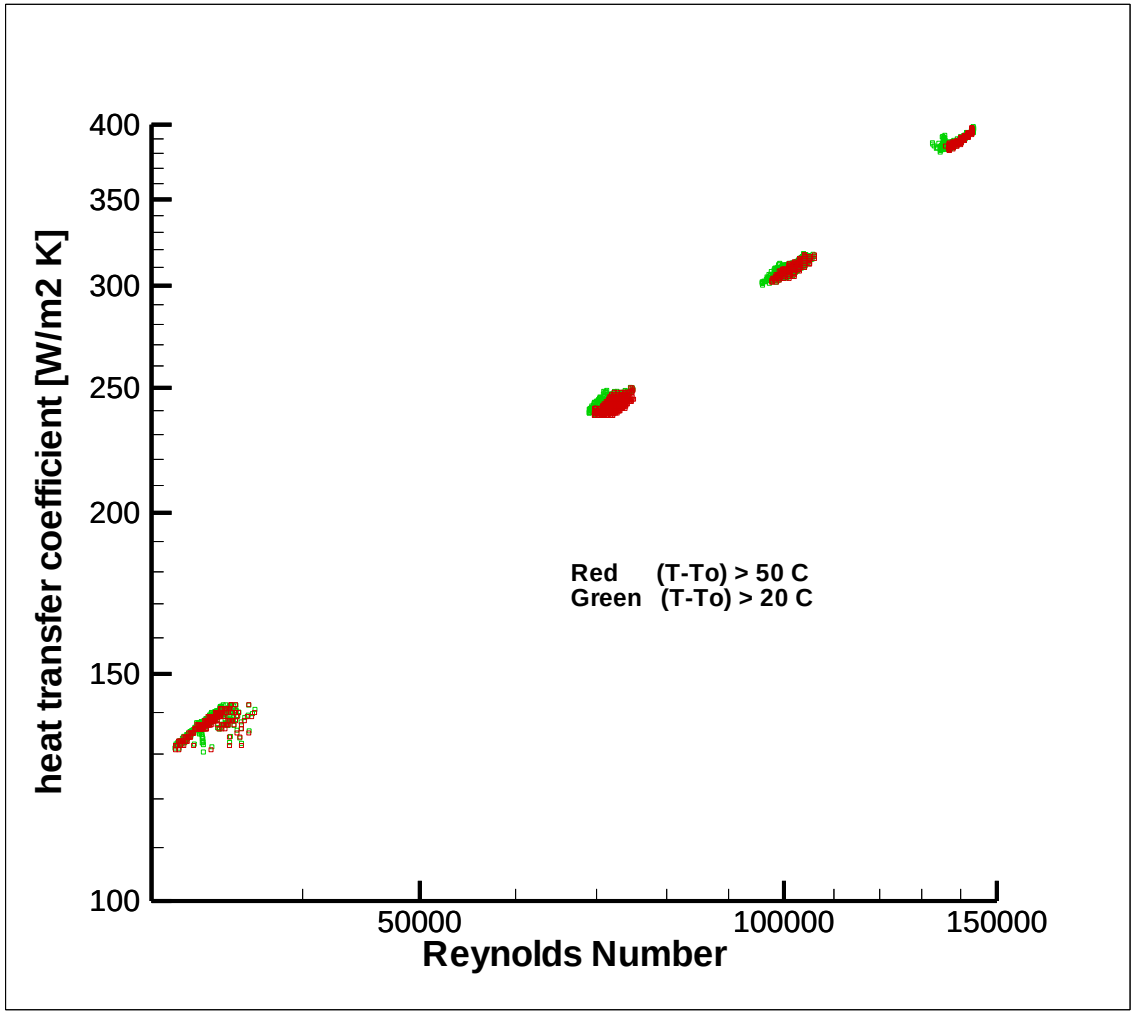

Figure 20: The Effect of the Cutoff Temperature on the Convective Heat Transfer Coefficient.

5 VALIDATIONS OF HEAT TRANSFER CORRELATIONS

5.1 METHOD

In order to validate the results from the testing phase it was necessary to create a second model. This model was developed to use the experimental data and the heat transfer correlations developed in the above work to predict probe temperature with time. The code, located in Appendix B of this document, reads in the experimental values for the time, T_0, mass flow, and power recorded every second by the data acquisition system. From these values the model calculates Reynolds number, heat transfer coefficient, and the new probe temperature. The calculated probe temperature can then be compared to the measured probe temperature.

Using the experimental data, Reynolds number can be calculated using Equation 4.4 in the form:

$$Re = \frac{md}{A_{d^*}\,\mu}$$

Using Equation 3.9:

$$h = 0.060Re^{0.743}$$

the heat transfer coefficient may also be calculated. Now with these data the change in temperature of the high temperature probe can be predicted using Equation 4.2 solved for dT/dt:

$$\frac{dT}{dt} = \left(\frac{EI}{C}\right) - \left(\frac{q_r}{C}\right) - \left(\frac{q_c}{C}\right) - \left(\left(\frac{Ah(T-T_0)}{C}\right)\right) \qquad \text{Equation 5.1}$$

A time-marching process was utilized where first a base point temperature for the high temperature probe (T) would need to be provided. The surrounding air temperature was selected to provide this base point to initialize the process. It follows that:

$$T_{probe} = T + \left(\frac{dT}{dt} * dt\right) \quad \text{Equation 5.2}$$

$$T = T_{probe} \quad \text{Equation 5.3}$$

The model will perform this iteration of equation 5.2 and 5.3 ten thousand times for each second of data and then write the result to the file. The results from this model and the experimental measurements using the correlations discussed above are plotted in Figure 21.

Note the differences in the peak temperatures for the measured probe data and the predicted data. This is a temperature difference of about 3.5 °C (roughly 4%), where the predicted temperature was overshooting the measured experimental temperature data in all but one instance, while the slope of the heating and cooling cycles remained on target. A parametric study was performed on the sensitivity of the predictive temperature code in an effort to isolate the cause of the temperature difference. The number of iterations was first modified from ten thousand (with a corresponding change in time step size) in order to verify that the model was converging on the new value for the probe temperature. This resulted in no change of the predicted temperature, and showed that the model had reached convergence.

The dT/dt coefficient (in equation 3.4) that was determined in the above text to be 42 J/°C was evaluated next. The coefficient was reduced and increased by 10% and then plotted with the measured temperature and original model predicted temperature in Figure 22. Evaluation of these curves shows that the slopes of the curves vary as a

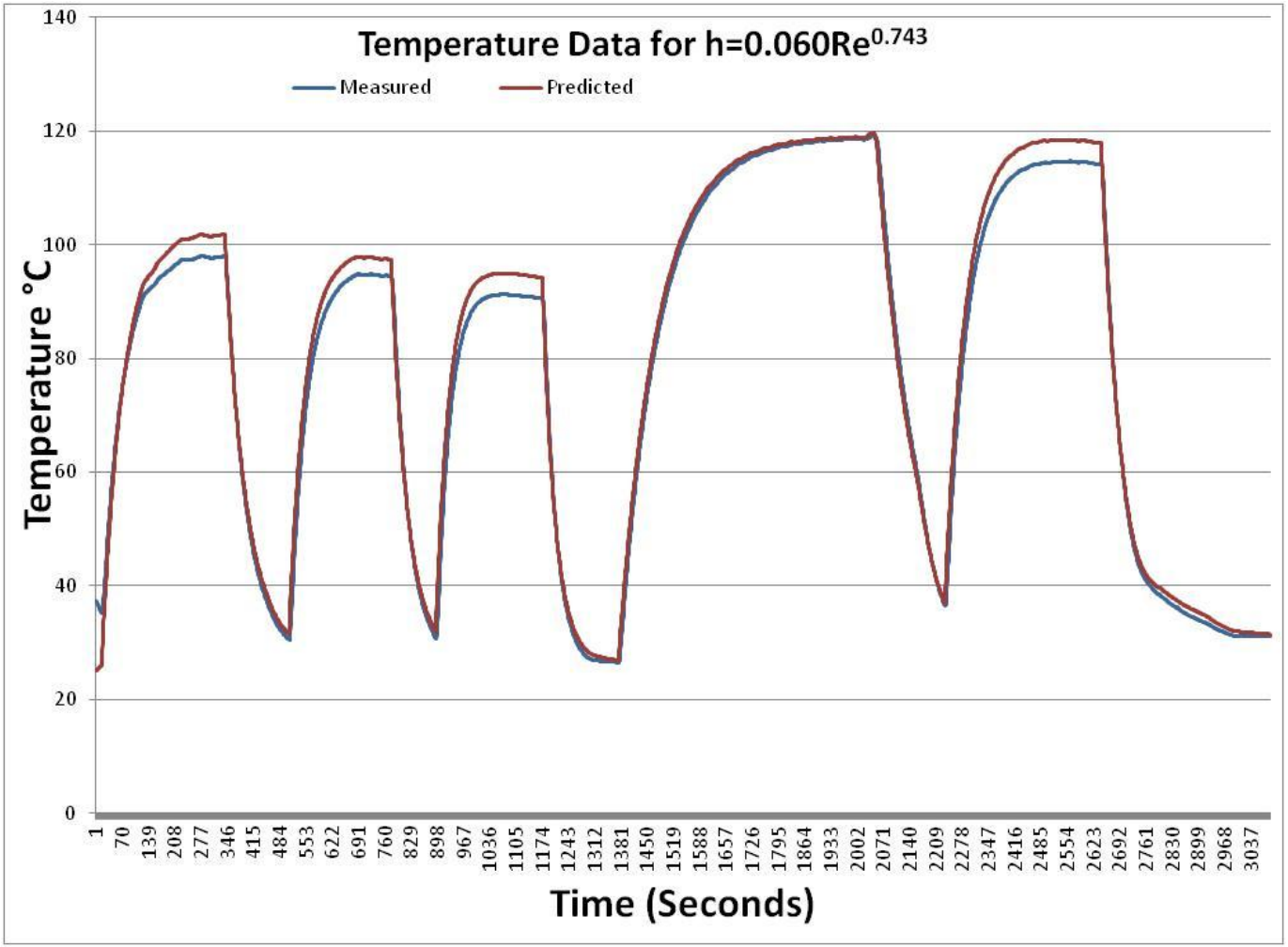

Figure 21: Plot of Predicted Probe Temperature Vs. Measured Temperature.

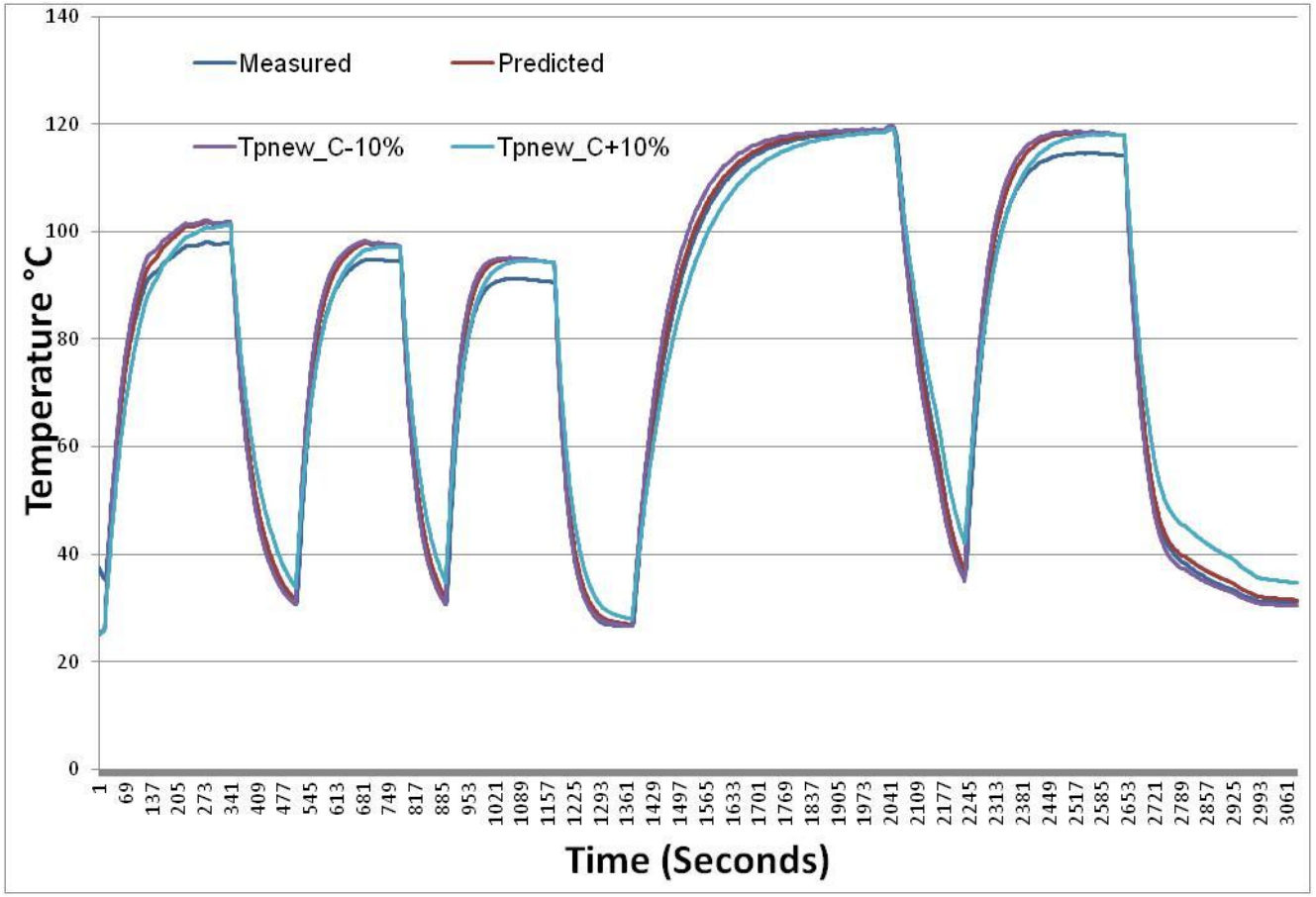

Figure 22: Temperature Model Results for dT/dt Coefficient ±10% vs. Predicted and Measured Temperature.

result of changing the coefficient values. While the slopes have variation, it has not affected the over shoot seen in the original predicted temperature results. This is expected when looking at Equation 5.1, the slope should increase and decrease inversely with the coefficient value.

It was determined that the values in Equation 3.8:

$$h = aRe^n$$

have the most influence on the overall shape of the curves. As described earlier, a least squares fit was performed on all of the heat transfer data which resulted in Equation 3.8, which has an uncertainty of 1.24%. The model was used to account for the ±1.24% difference in h when calculating the predicted probe temperature. This created a band in which the measured temperatures should fall. These data are plotted in Figure 23. Again, only one data set seems to fall in the acceptable band for the stated accuracy of the derived correlation.

It was observed that by modifying the value for a the maximum temperature reached could be shifted, while preserving the slopes for the heating and cooling cycles. By iterating a it was determined that $a = 0.063$ produces predicted values for the probe temperature for four of the five data sets that are within the range of uncertainty. This can be seen in Figure 24. The data set that deviates from this trend is unique in the fact that it is the only case in which there is a low mass flow and low Reynolds number condition when compared to the other data points.

It is important to mention that the data being presented is a small cross section of the total data gathered and that the correlations presented were developed using the whole of all the data sets. Also recall that these correlations were derived from a least squares fit of all of the heat transfer data. It is the opinion of the author that the

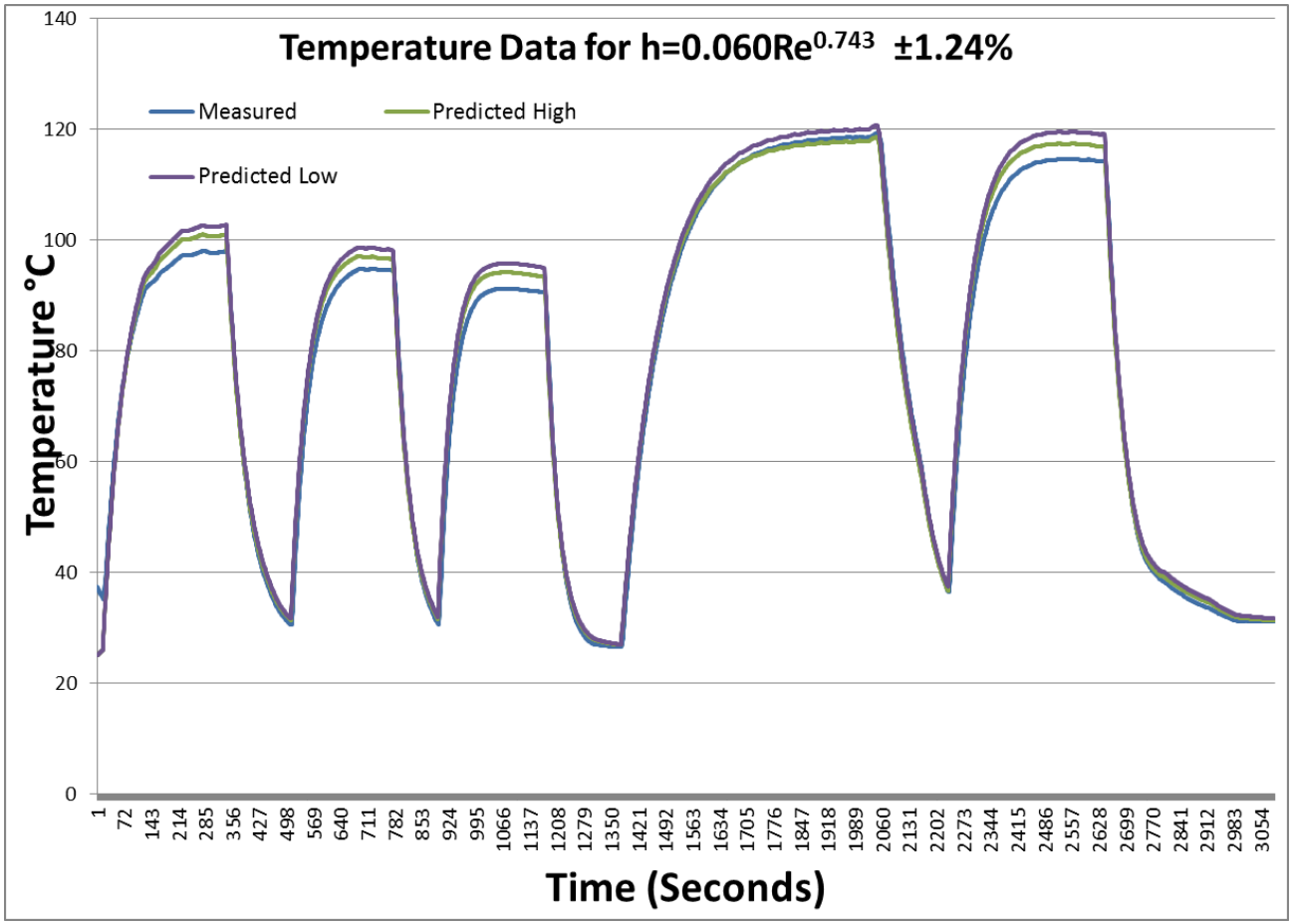

Figure 23: Temperature Vs. Time Including the Uncertainty of ±1.24%.

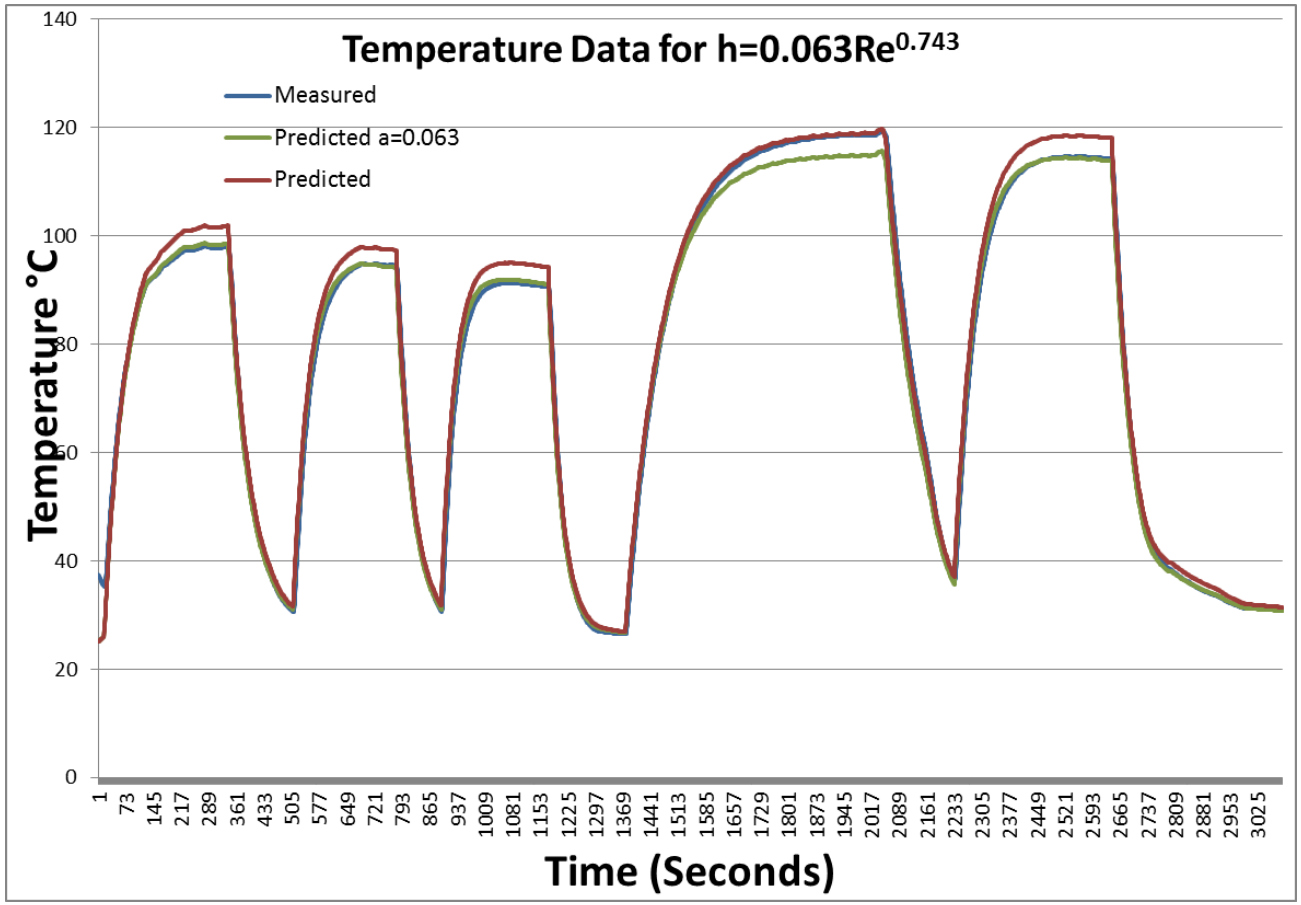

Figure 24: Temperature Vs. Time for Measured and Predicted data.

uncertainties associated with Equation 3.9 are not adequate for all ranges of the data. It is recommended to only use the correlations within the range of stated test conditions.

5.2 EVALUATION OF THE CONSTANT C

As described in Section 3.1, the lumped constant C was determined previously to be 42 J/°C using data gathered during testing in the test facility with air flowing. Because this value of C was determined using transient data projected to steady state, experimental confirmation of the resulting value of C is desired. An attempt was made to evaluate this constant using the insulated, heater and assembled high temperature probe, data in order to further validate this value. Again by adding equations 3.1 and 3.2 the unmeasured heater temperature (T_h) and the effective conductivity (k) of the interface between the heater and the shell are eliminated. Since the data from the insulated cases were used, it is assumed that heat loss by convection (q_c) and radiation (q_r) may be eliminated. This leaves:

$$C = \frac{(EI - q_{cond})dt}{dT_h - dT} \qquad \text{Equation 5.3}$$

where again C is a constant approximately equal to $(\rho V Cp + \rho_h V_h Cp_h)$. The change in temperature for the heater and the assembled high temperature probe are (dT_h) and (dT) respectfully for each time step. Three runs were evaluated, and the results may be seen in the Table 9.

Table 9: Evaluation of the C constant using insulated probe test data.

Run 1		Run 2		Run 3	
	C (J/°C)		C (J/°C)		C (J/°C)
Min.	32.9	Min.	31.5	Min.	33.1
Max	46.5	Max	47.31	Max	45.25
Average	37.5	Average	38.2	Average	37.9

The values for C remained relatively constant for the different power and temperature ranges, but does not reach 42 J/°C calculated with the from the air on tests. This represents an 8.3% discrepancy between the value calculated for the air on and insulated tests, which warrants further assessment and discussion. For the air-on test runs (in the presence of flowing air), noise in the temperature data caused by the inability of the facility flow valve to actively control mass flow led to averaging the derivative term (*dT/dt*) over a range of data points (Equation 3.6). For the insulated case this averaging did not occur. Plotting the temperature of the probe with respect to time, in Figure 25, for the insulated case shows that the slope of the heating cycle appears to be linear for each trial, for temperatures above 50 C. For the cooling cycle the slope decreases as the probe approaches the temperature of the surrounding environment. This is to be expected due to the heat loss via conduction through the copper leads of the heater. This rate of heat transfer is directly proportional to the ΔT between the hot and cold environment. It was also assumed that the convection and radiation heat loss terms could be eliminated for the insulated cases; if not correct these terms could increase the heat loss experienced by the heater. Figures 25 and 26 show C as a function of measured temperature and power input to the heater, respectively. As seen in Table 9, and Figures 25 and 26, it is clear that there is a wide range of C values for the insulated test case. Recall that we expect C to be constant.

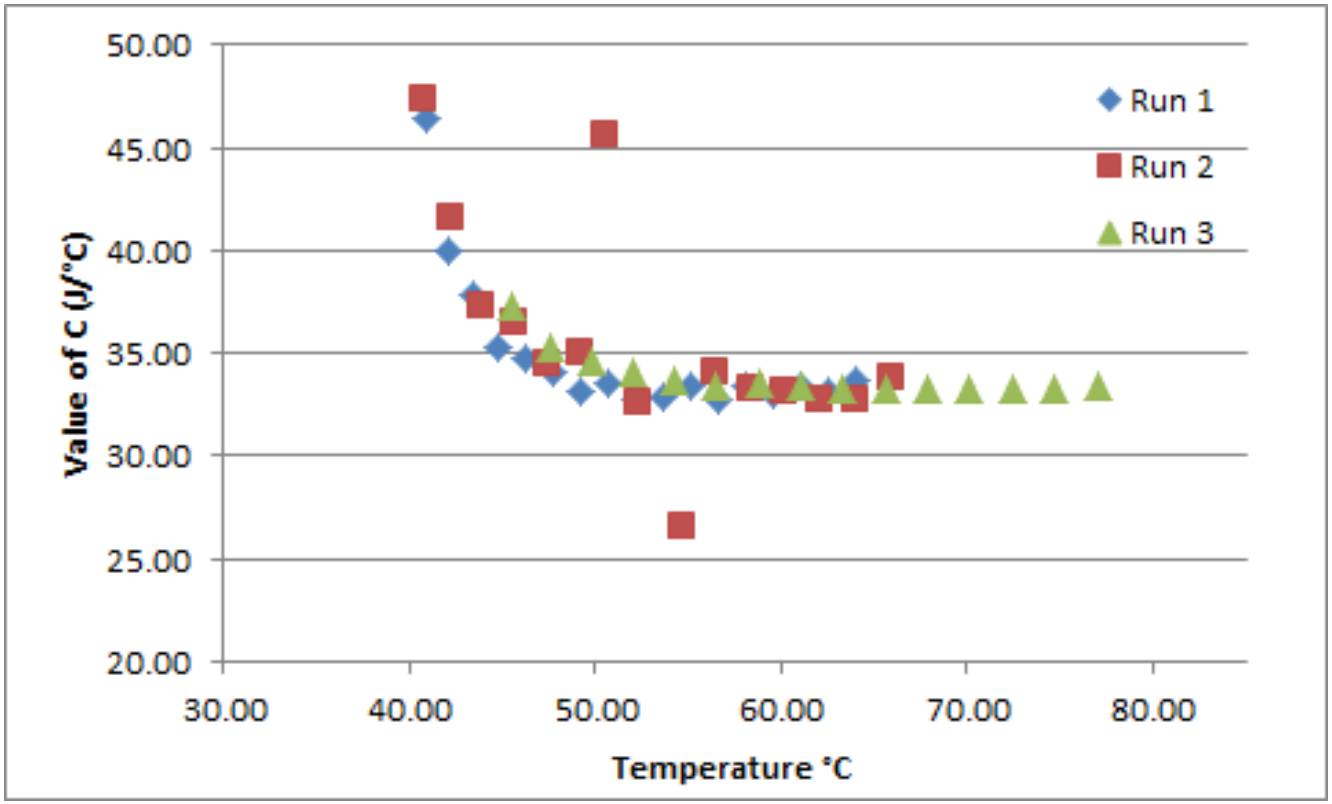

Figure 25: Values of C vs. Temperature.

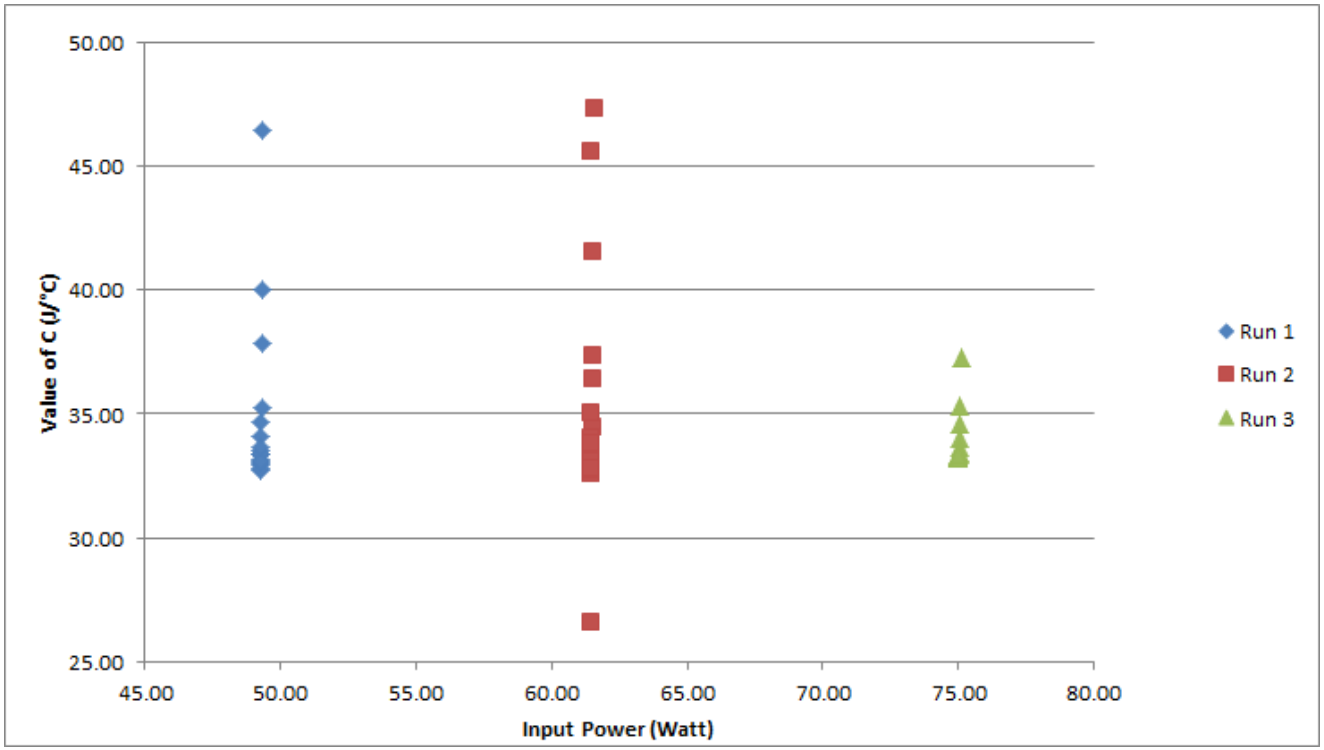

Figure 26: Value of C vs. Input Power.

Examining Figure 26, it can be seen that the value of C was the most consistent for the run with the highest input power setting, Run 3. This result can be explained by again looking at Equation 5.3, repeated here for convenience:

$$C = \frac{(EI - q_{cond})dt}{dT_h - dT}$$

The derivative terms (dT_h/dt) and (dT/dt) are the change in temperature for the heating and cooling cycles respectively of each time interval. At the higher input power (EI) settings the heating slope increases very rapidly with time and does not reach an equilibrium state. Therefore the slope of the line changes very little. Since all other terms in the equation remain relatively constant, the results for C in Equation 5.3 are dominated by the difference of the slopes for the heating and cooling cycles.

6 CONCLUSIONS

6.1 HEAT TRANSFER CORRELATION WITH UNCERTAINITES

A least square fit of all of the heat transfer data results in the heat transfer / Reynolds number relationship of:

$$h = 0.060Re^{0.743} \text{ (with an uncertainty of 1.24\%)} \qquad \text{Equation 6.1}$$

for 30,000 < Re < 150,000

All of this data was taken on a 0.0254 m (1 in) diameter probe in 25 °C air with a thermal conductivity (*k*) of 0.024 W/m°C and a Prandtl number (*Pr*) of 0.71. It is noted that this relationship does not account for changes in gas properties or the probe diameter; therefore, it should not be used for flow conditions that vary significantly from those specified. To provide this capability, a Nusselt number correlation is required.

6.2 NUSSELT CORRELATION WITH UNCERTAINTIES

The Nusselt number (*hd/k*) is proportional to the product of the Reynolds and Prandtl numbers, each raised to some power. The experiments conducted in this work do not have any significant variation in Prandtl number, and the correlation with Nusselt number assumes the functional form from a cylinder in cross flow for which the Prandtl number is raised to the 1/3 power. With the assumption that the Nusselt number will fit the functional form $Nu = a\,Re^{n}\,Pr^{1/3}$, the relation for *Nu* was found to be:

$$Nu = \frac{hD}{k} = 0.071 Re^{0.743} Pr^{\frac{1}{3}}$$ (with an uncertainty of 1.86%) Equation 6.2

for 30,000 < Re < 150,000

6.3 EFFECTS OF TURBULENCE

For the range of relative turbulence levels (3% to 14%) realized in the tests, the convective heat transfer coefficients agree within uncertainty.

6.4 EFFECTS OF POWER ($T-T_0$)

For the range of $T-T_o$ levels (71 to 88 K) realized in the tests, the convective heat transfer coefficients agree within uncertainty.

6.5 EFFECT OF PENETRATION DEPTH

Tests were conducted for two penetration depths, 1.8 inches and 3 inches. The former is the penetration depth selected for a high-temperature measuring probe in a high temperature environment, scaled to the six inch pipe used for this study. Note that the velocity profile determined from swept total pressure measurements indicates that 1.8 inches from the wall is within the boundary layer. The latter was selected to ensure that measurements were made outside of the boundary layer. Results indicate a slight increase in Nu that results from the higher velocities realized outside of the boundary layer.

6.6 VALIDATIONS OF HEAT TRANSFER CORRELATIONS

C should not vary significantly for the narrow temperature range realized during these tests—invalidating these test cases. Potential causes for this poor test data include: (1) a thermal insulator that permits conduction losses that are too high, (2) heater power

and thermocouple lead conduction losses that are significantly underestimated, (3) data for cases where the rate of heating was not constant were evaluated.

In conclusion it is the recommendation of the author that testing be repeated with further work be done to eliminate the fluctuations of mass flow by adding a control valve with active flow control. This would largely eliminate the cyclic change in the temperature seen in the data and would allow the averaging in equation 3.6 to be eliminated. Also the insulator used for the insulated test case should be evaluated to verify that heat losses due to (q_c) and (q_r) are negligible.

BIBLIOGRAPHY

Anderson, J. D. (2003). *Modern Compressible Flow with Historical Perspective.* New York: McGraw-Hill.

Bejan, A., & Kraus, A. D. (2003). *Heat Transfer Handbook.* Jefferson City: Wiley & Sons.

Bergman, T. L., Dewitt, D. P., Incropera, F. P., & Lavine, A. S. (2011). *Fundamentals of Heat and Mass Transfer.* Jefferson City: Wiley & Sons.

Engineering Toolbox. (n.d.). Retrieved March 5, 2013, from "Emissivity Coefficients for some Common Materials": http://www.engineeringtoolbox.com/emissivity-coefficients-d_447.html

Gordon, S., & McBride, B. J. (1994). *Computer Program for Calculation of Complex Chemical Equilibrium Compositions and Applications.* NASA Reference Publication 1311.

Incropera, F. P., & Dewitt, D. P. (1990). *Fundamentals of Heat and Mass Transfer, 3 rd Ed.* Jefferson City: Wiley & Sons.

Sutherland, W. (1893). The Viscosity of Gases and Molecular Force. *Philosophical Magazine*, pp. 507-531.

APPENDICES

APPENDIX A

Venturi Flowmeter

FlowDyne® Venturi Flowmeter

PN: VPO41563-SF

SN: 18982

D1 diameter = 4.012”, D2 diameter = 1.5615”

Venturi High Pressure Transducer

Type: Omega® Thin-Film Polysilicon Pressure Transmitter

PN: PX615-150G1

Range: 0-150 PSIG

Output: 4-20mA

Accuracy: +/-0.4% BFSL

Hysteresis: +/-0.2%

Repeatability: +/-0.07%

Stability: +/-0.5%/year

Thermal Zero Effect: +/-0.07% FS/°C

Thermal Span Effect: +/-0.07% FS/°C

Venturi Differential

Type: Rosemont® Alphaline Differential Pressure Transmitter®

Model: 1151DP6E12D3

SN: 252740

Range: 0-50 PSID

Output: 4-20mA

Accuracy: +/-0.25% of calibrated span

Stability: +/-25% of upper range limit (URL)

Thermal Zero Effect: +/-0.5% per 100°F

Thermal Span Effect: (+/-0.5% URL + 0.5% of calibrated span) per 100°F

Static Pressure Zero Error: +/-2.5% of URL for 2,000 psi

Static Pressure Span Error 0.25% of input reading per 1,000 psi

Stilling Pressure

Type: Rosemont® Alphaline Differential Pressure Transmitter®

Model: 1151P5E12B1

Range: 0-20 PSID

Output: 4-20mA

Accuracy: +/-0.25% of calibrated span

Stability: +/-25% of upper range limit (URL)

Thermal Zero Effect: +/-0.5% per 100°F

Thermal Span Effect: (+/-0.5% URL + 0.5% of calibrated span) per 100°F

Static Pressure Zero Error: +/-2.5% of URL for 2,000 psi

Static Pressure Span Error 0.25% of input reading per 1,000 psi

Pitot Pressure

Type: Rosemont® Alphaline Differential Pressure Transmitter®

Model: 1151DP4E12B1

Range: 0-5 PSID

Output: 4-20mA

Accuracy: +/-0.25% of calibrated span

Stability: +/-25% of upper range limit (URL)

Thermal Zero Effect: +/-0.5% per 100°F

Thermal Span Effect: (+/-0.5% URL + 0.5% of calibrated span) per 100°F

Static Pressure Zero Error: +/-2.5% of URL for 2,000 psi

Static Pressure Span Error 0.25% of input reading per 1,000 psi

Static Pressure

Type: Setra®

Model: 264

Part #: 2641005WD2DTT1G

Range: 0-5” WC

Output: 0-5 VDC

Accuracy: +/-0.25% of calibrated span

Stability: +/-25% of upper range limit (URL)

Thermal Zero Effect: +/-0.5% per 100°F

Thermal Span Effect: (+/-0.5% URL + 0.5% of calibrated span) per 100°F

Static Pressure Zero Error: +/-2.5% of URL for 2,000 psi

Static Pressure Span Error 0.25% of input reading per 1,000 psi

Thermocouples

Manufacturer: Omega®

Model: KMQXL-062G-12 sub min t/C w/molded connector

Type: K - grounded

Diameter: 0.062”

Length 12”

Temperature Drift: less than 2.8°C in 25 weeks typical

Cartridge Heater

Type: McMaster-Carr Part#3614K51

Rating: 120V, 3/8# diameter, 1” length, 100 watts

Comments: Bonded graphite coating. Magnesium oxide insulation in incoloy sheath

Max Temp: 1600°F

Power Supply

Type: HP6483A 0-600VDC/0-25A power supply

SN: 1921A00211

Load Regulation: less than 0.05% plus 100mV

Ripple and Noise: less than 600mVrms, 5Vp-p

Temperature Coefficient: less than 0.03% plus 20mV change in output per degree C

Stability: less than 0.15% plus 80- mV total drift per 8 hours under constant ambient conditions

Resolution: 60 mV

Calibration Multimeter

Type: Fluke® 8840A 5.5 digit, true RMS multimeter

SN: 3773093

DC Voltage Resolution:

200 mV range: 1 uV

2 V range: 10 uV

20 V range: 100 uV

200 V range: 1 mV

1000 V range: 10 mV

DC Voltage Accuracy:

200 mV range: +/- 0.003% of reading

2 V range: +/-0.002% of reading

20 V range: +/-0.002% of reading

200 V range: +/- 0.002% of reading

1000 V range: +/- 0.003% of reading

DC Current Resolution

2000mA Range: 10 uA

DC Current Accuracy:

Less than 1 A: 0.04 % of reading

Greater than 1 A: 0.1 % of reading

Calibration Precision Digital Thermometer

Type: Guildline® Model 9540A Precision Digital Thermometer®

SN: 61 427

Range: -20°C - +60°C

Resolution: 0.001°C

Limits of Error: +/- 0.05°C

Temperature coefficient: less than 0.0005°C/°C

Pressure Calibrator

Type: Druck® DPI 601

Combined non-linearity, hysteresis and repeatability: +/- 0.05% FS

Temperature Effects on Span: +/- 0.3% FS

Constant Temperature Anemometer

Manufacturer: TSI®

Model: IFA-300

SN: 327D

Software: ThermalPro version 2.25

A/D card resolution: 12bit

Signal Conditioner Offset Accuracy : +/-0.15% Accuracy

Signal Conditioner Gain Accuracy: +/- 0.15%

Amplifier Drift: 0.3 uV/°C

Amplifier Input Noise: 1.7 nV/sqrt(Hz) & 1.5pA/ sqrt(Hz)

Sample Rate: 10,000 Hz

Size: 128 Kpts/ch

Time: 13.1072 sec

Data Acquisition System

Data Acquisition Card

Manufacturer: National Instruments®

Model: PCI-6221

ADC resolution: 16 bits

Nominal Range+/-0.2 V

Absolute Accuracy at Full Scale: 112 uV

Sensitivity: 5.2 uV

Random Noise: 13 uVrms

Noise Uncertainty: RandomNoise*3/sqrt(100)

Nominal Range+/-1.0 V

Absolute Accuracy at Full Scale: 360 uV

Sensitivity: 12 uV

Random Noise: 30 uVrms

Noise Uncertainty: RandomNoise*3/sqrt(100)

Nominal Range+/-5.0 V

Absolute Accuracy at Full Scale: 1620 uV

Sensitivity: 48.8 uV

Random Noise: 122 uVrms

Noise Uncertainty: RandomNoise*3/sqrt(100)

Nominal Range+/-10.0 V

Absolute Accuracy at Full Scale: 3100 uV

Sensitivity: 97.6 uV

Random Noise: 244 uVrms

Noise Uncertainty: RandomNoise*3/sqrt(100)

Signal Conditioner Card

Chassis Type: National Instruments® SCXI-1000

Signal Conditioner Card: National Instruments SCXI-1102C

Signal Conditioner Card Terminal Block: National Instruments SCXI-1303

Nominal Range+/-100mV

Accuracy: .015 % of reading typical, .02% max

System Noise (peak 3 sigma): 30uV

Temperature Drift: 0 .0005 % of reading/ °C

Nominal Range+/-10V

Accuracy: .025 % of reading typical, .035% max

System Noise (peak 3 sigma): 600uV

Temperature Drift: 0 .0010 % of reading/ °C

Materials List:

Probe Insulating Foam (used between probe and support tube and inside support tube)

Alumilite Super foam 320

Release Agent (used to coat aluminum mold for foam insulation)

Synair Synlube 1711 Release Agent

Thermal Grease (applied to cartridge heater)

Omega Engineering Omegatherm “201” high temperature Conductivity Paste

Glue (used to secure thermocouples into probe)

Loctite Gel Control Super Glue

APPENDIX B

```
Program sort

      dimension V(27) !number of columes
      parameter(pi=3.14159)
      real*8 mdot, T_pold, power, T_pnew, thea, C, T0, Tchg

      open(unit=24,file="Envornment_Data_in.txt",status='old',action='read')  !Change the name of the input
file to match one being used
      open(unit=25,file="sort_out.txt",status='replace',action='write') !opens output file to write to.
      open(unit=26,file="Re_test.txt",status='replace',action='write')
      write(26,'(6A15)') "d_probe", "mdot", "d_duct", "A_duct", "Visc_air", "Re", "h"

      read(24,'(A)') !moves read from line 1 to line 2
      write(25,'(7A15)') "Time", "T_0", "Mdot", "Power", "Re", "h", "Tpnew" !Colume Headers. Changes
depending on what you want from line write statement below
      T_pold=25
      do j=1,3089 !Number of (rows - 1) (Change to match the input file being used)
      read(24,*) (V(I), I=1,27) !I is the number of columes (Change to match the input file being used)


      d_probe=1.000 !diameter of probe in inches
      mdot=V(24)  !mass flow in english units (lbm/s)
      d_duct=6.005 !diameter in inches

      !convert to SI
      d_probe=d_probe*0.0254 !converts to meters (SI)
      mdot= mdot*0.453592 !converts from lbm/s to kg/s (SI)
      d_duct=d_duct*0.0254 !converts to meters(SI)

      A_duct = ((d_duct**2)*pi)/4 !units SI (m^2)
      Visc_air=1.983E-5 !from table 100F (Kg/m*s)
      Re =(mdot*d_probe)/(A_duct*Visc_air)
      h = (0.063)*(Re**0.743) ! default value is (0.060)
      !!!!!!!!!!!!!!!!!!!!!!!!!!!!!!!!!!!!!!!!!!!!!!   Insert Probe Temp calculation    !!!!!!!!!!!!!!!!!!!!!!!!
      A_psurf=((pi*(d_probe**2))/4)+(pi*d_probe*(1.25*0.0254)) !units  m^2
      thea=5.667E-8
      power=V(27)
      C=42 !  default value is (42)  units J/degree C
      dt=.001
      T0=V(18)
      emis=.10 ! default value is (.10)
      do I=1,1000
        qr=5.667E-8*A_psurf*emis*(((T_pold+272.15)**4)-((T0+272.15)**4))!units Watt
        qc=0.021*(T_pold-T0) !units Watt
        T_chg=((power/C)-(qr/C)-(qc/C)-((A_psurf*h*(T_pold-T0))/C))
        T_pnew=T_pold+(T_chg*dt)
        T_pold=T_pnew
```

```
        enddo

      write(26,'(6E15.6)') d_probe, mdot, d_duct, A_duct, Visc_air, Re, h
      write(25,'(7E15.6)') V(1),V(18),V(24),V(27),Re, h, T_pnew !picks out the columes that you need
(Change based on input file being used)
      enddo
      close(unit=24) !closes the input file
      close(unit=25) !closes the output file
      close(unit=26)
      stop
      endprogram sort
```

VITA

Marcus Conner was born in Waterloo, IA, to the parents of Janet Davis and Donald Conner. He is the last of four children: April, Adam, and Matthew. Marcus and his family moved to Smyrna, TN before his first birthday. He graduated from Smyrna High School. Throughout childhood he showed interest in model aviation. After graduation these interests lead him to pursue a degree in Mechanical Engineering. In 2008 he graduated from Tennessee Technological University (TTU) with his undergraduate degree. While in college at TTU Marcus meet his future wife, now Mrs. Courtney Conner. They have one child Mr. Laim Conner. After graduation from college he pursued a career in Engineering at Arnold Engineering Development Center (AEDC), one of the world's premier aerospace testing facilities. While working at AEDC Marcus enrolled in graduate course work at the University of Tennessee Space Institute. The work completed in this document will satisfy his requirements for a Master of Science degree in Mechanical Engineering.